

PAPER • OPEN ACCESS

Fractional Brownian motion with random diffusivity: emerging residual nonergodicity below the correlation time

To cite this article: Wei Wang *et al* 2020 *J. Phys. A: Math. Theor.* **53** 474001

View the [article online](#) for updates and enhancements.



IOP | ebooks™

Bringing together innovative digital publishing with leading authors from the global scientific community.

Start exploring the collection—download the first chapter of every title for free.

Fractional Brownian motion with random diffusivity: emerging residual nonergodicity below the correlation time

Wei Wang^{1,2,5}, Andrey G Cherstvy², Aleksei V Chechkin^{2,3}, Samudrajit Thapa², Flavio Seno⁴, Xianbin Liu¹ and Ralf Metzler^{2,*}

¹ College of Aerospace Engineering, Nanjing University of Aeronautics and Astronautics, 210016 Nanjing, People's Republic of China

² Institute for Physics & Astronomy, University of Potsdam, 14476 Potsdam-Golm, Germany

³ Institute for Theoretical Physics, Kharkov Institute of Physics and Technology, 61108 Kharkov, Ukraine

⁴ INFN (Padova Section) and Department of Physics and Astronomy 'G. Galilei', University of Padova, 35122 Padova, Italy

⁵ Max-Planck Institute for the Physics of Complex Systems, Nöthnitzer Str. 38, D-01187 Dresden, Germany

E-mail: rmetzler@uni-potsdam.de

Received 19 April 2020, revised 29 June 2020

Accepted for publication 9 July 2020

Published 4 November 2020



CrossMark

Abstract

Numerous examples for *a priori* unexpected non-Gaussian behaviour for normal and anomalous diffusion have recently been reported in single-particle tracking experiments. Here, we address the case of non-Gaussian anomalous diffusion in terms of a random-diffusivity mechanism in the presence of power-law correlated fractional Gaussian noise. We study the ergodic properties of this model via examining the ensemble- and time-averaged mean-squared displacements as well as the ergodicity breaking parameter EB quantifying the trajectory-to-trajectory fluctuations of the latter. For long measurement times, interesting crossover behaviour is found as function of the correlation time τ characterising the diffusivity dynamics. We unveil that at short lag times the EB parameter reaches a universal plateau. The corresponding residual value of EB is shown to depend only on τ and the trajectory length. The EB parameter at long lag times, however, follows the same power-law scaling as for fractional Brownian motion. We also determine a

* Author to whom any correspondence should be addressed.



Original content from this work may be used under the terms of the [Creative Commons Attribution 4.0 licence](https://creativecommons.org/licenses/by/4.0/). Any further distribution of this work must maintain attribution to the author(s) and the title of the work, journal citation and DOI.

corresponding plateau at short lag times for the *discrete* representation of fractional Brownian motion, absent in the continuous-time formulation. These analytical predictions are in excellent agreement with results of computer simulations of the underlying stochastic processes. Our findings can help distinguishing and categorising certain nonergodic and non-Gaussian features of particle displacements, as observed in recent single-particle tracking experiments.

Keywords: stochastic processes, anomalous diffusion, fractional Brownian motion, diffusing diffusivity, weak ergodicity breaking

(Some figures may appear in colour only in the online journal)

1. Introduction

Brownian motion (BM) describes ubiquitous physical phenomena across multiple disciplines of natural science. Based on multiple experimental findings and theoretical frameworks [1–10], BM features two fundamental properties: (i) the linear growth of the mean-squared displacement (MSD) with time and (ii) the Gaussian form of the probability density function (PDF) of particle displacements. Anomalous diffusion processes feature a nonlinear MSD growth, typically of the power-law form [11–22]

$$\langle x^2(t) \rangle \propto t^{2H}. \quad (1)$$

Subdiffusion is observed when the anomalous scaling exponent is in the range $0 < H < 1/2$, while superdiffusion is realised for $1/2 < H < 1$. Especially, prompted by modern technologies (such as superresolution microscopy, fluorescence technologies, single-particle tracking and advanced computing methods), anomalous diffusion has been detected in numerous physical and biological systems [18, 24–33]. Along with these experimental developments, the mathematical foundations of different models of anomalous diffusion have been intensively studied, such as, for instance, for continuous-time random walks [14, 19, 34–36], fractional BM (FBM) [37–44] (also with tempered noise [45, 46]), and heterogeneous diffusion processes [47–53].

Over the past years, a particular class of stochastic processes—so-called ‘Brownian yet non-Gaussian diffusion’—has been reported in a representative number of soft-matter and cellular biological systems [54–64]. These processes typically combine the linear BM-like growth of the MSD with a highly non-Gaussian (often close to exponential) PDF of particle displacements for given time lags. These non-Gaussian PDFs may emerge due to diffusion in inhomogeneous environments. In a first approach it was assumed that each particle is moving on a spatial patch with a given diffusivity, D . Measuring the displacement-PDF of an ensemble of particles, imagined to be distributed over a set of local patches, is then taken to be a weighted mean of individual Gaussians with a given diffusion coefficient, where the weight function is the PDF $p(D)$ of diffusion coefficients. This is, in fact, the classical approach of ‘superstatistics’ [65, 66]. For instance, in the experiment of Granick and coworkers, for colloidal beads diffusing on lipid-bilayer tubes an exponential distribution $p(D)$ was obtained [54, 55]. However, the superstatistical model with time-independent $p(D)$ cannot predict the crossover from short-time non-Gaussian to long-time effective Gaussian PDFs observed experimentally [54, 55].

To allow for such a crossover, the concept of ‘diffusing diffusivity’ (DD) was introduced [67]. Introducing a fluctuating instantaneous $D(t)$, in this model exponential PDFs at short times and Gaussian PDFs at long times emerge, while the process still features a linear MSD

with time-independent effective diffusivity. The crossover is characterised by the correlation time inherent to the diffusivity dynamics. A similar concept of distributed diffusivities was previously developed in reference [68] (see also reference [69]). The DD approach helps mimicking and rationalising the impact of static and dynamical heterogeneities [70–75] on various statistical quantifiers of the particle-spreading dynamics.

Recently, various modifications and extensions of the DD model [67] were developed [76–98]. Specifically, a minimal DD model [87] provided the general analytical subordination-based framework for Brownian yet non-Gaussian processes. Persistent and antipersistent anomalous diffusion processes of FBM of generalised-master-equation family are normally also Gaussian. However, antipersistent non-Gaussian dynamics have been observed as well [99, 100].

To accommodate this dynamics, recent advances of the DD model include the superstatistical FBM approach [99] describing the exponential PDFs as observed, e.g., for cytoplasmic RNA-protein diffusion in bacterial and eukaryotic cells [99]. A more general approach for the superstatistical generalised Langevin equation was developed in reference [101]. The link between the DD model and random-coefficient autoregressive model for non-Gaussian diffusion was established [102] and a DD model for generalised grey BM was developed [88].

Strongly non-Gaussian behaviours were reported for a number of complex systems, such as, e.g., molecular diffusion of lipid molecules or proteins embedded in protein-crowded lipid membranes [100, 103, 104], dynamics of polymers transiently adsorbed at solid–liquid interfaces [106, 107], spreading dynamics of micron-size tracers in mucin-polymer gels [105, 108], transiently superdiffusive spreading of amoeboid cells in heterogeneous populations [109], anomalous transport of tracers in amoeboid cells [110], dynamics of colloidal particles near a wall [111], in dense matrices of micropillars [71] and anisotropic liquid crystals [112], diffusion in narrow corrugated channels with fluctuating cross-sections [113], and the dynamics of acetylcholine receptors on live muscle-cell membranes [114].

The paper is organised as follows. In section 2 we introduce the physical observables used in the description and the basic equations solved in the text. In sections 3.1 and 3.2 the time-averaged MSD (TAMSD) and the EB parameter of the DD-FBM model, respectively, are calculated analytically and supported by the results of computer simulations. We provide analytical expressions for EB for the BM case $H = 1/2$ and numerical results for the whole range $H \in (0, 1)$. The discussion and conclusions are summarised in section 4.

2. Physical observables and formulation of the DD model

2.1. Ensemble- versus time-averaging

Single-particle tracking (SPT) routinely measures the trajectories of submicron or even single-molecular tracers in the form of time series of the particle position at unprecedented spatial and temporal resolution. SPT is by now an established powerful tool to study ‘microscopic’ diffusion in a broad spectrum of physical systems at different length- and time-scales. For a large number of SPT trajectories, the ensemble-based MSD is a well suited statistical measure. The dynamics is, however, often assessed from a limited number of long SPT trajectories in terms of the TAMSD. In accord with the ergodic hypothesis [19], the TAMSD for a given trajectory of a particle exploring the entire system for long times is equivalent to the MSD computed for a large ensemble of identical particles diffusing in the same system. In contrast, when the system features weak ergodicity breaking [115, 116] the MSD and TAMSD cease to coincide, even for long measurement times T [16, 19]. However, even for ergodic processes an ensemble of TAMSDs features a finite spread for finite trajectories. This spread is

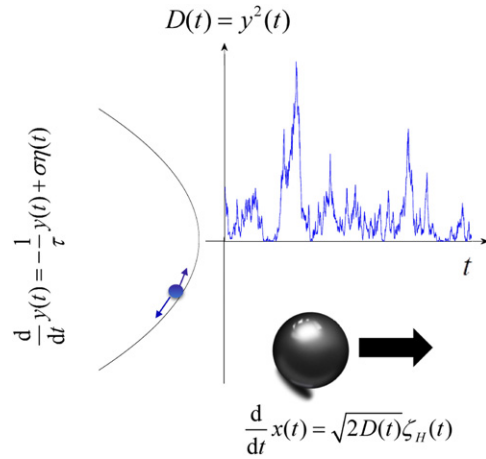


Figure 1. Physical interpretation and schematic of the DD-FBM diffusion model. The position $x(t)$ is driven by fractional Gaussian noise $\zeta_H(t)$, whose amplitude is modulated by stochastic diffusivity $D(t)$. The latter is taken to be the square of the Ornstein-Uhlenbeck process $y(t)$.

quantified by EB, which has been studied for many normal and anomalous stochastic processes [19, 29, 39, 44, 117–121].

The normal-diffusion DD model [87] and the DD-FBM model driven by power-law correlated noise $\zeta_H(t)$ [38, 39] are central for the current study, see figure 1. The ergodic properties of the DD-FBM process—defined below in the Boltzmann–Khinchin sense of the equivalence of the long-time limit of the MSD (2) and TAMSD (3) [16, 19, 121]—are investigated via analysing the realisation-to-realisation amplitude variation of individual TAMSDs quantified by EB, see equation (6) below. This is also a practical definition of ergodicity used, for instance, in statistical physics dealing with SPT data, as experimentalists often measure time averages. We do not talk about rigorous conditions of ergodicity, for instance, in the sense discussed in reference [122]. A detailed comparison of the dynamics and the (non-)ergodicity to the behaviours of pure FBM and the DD model is provided and the discrepancies are quantified below. In particular, we identify a fundamental time-scale below which EB features a plateau and we determine the residual EB value.

2.2. Definition of main observables

The MSD—the standard observable for a stochastic process [16–19]—is the average of the squared particle position with the PDF of its displacements at time t ,

$$\langle x^2(t) \rangle = \int_{-\infty}^{+\infty} x^2 P(x, t) dx. \quad (2)$$

Here and below we consider one-dimensional systems; component-wise extension to higher dimensions is possible. The TAMSD for a time series $x_i(t)$ of the i th particle is typically defined as

$$\overline{\delta_i^2(\Delta)} = \frac{1}{T - \Delta} \int_0^{T-\Delta} [x_i(t + \Delta) - x_i(t)]^2 dt, \quad (3)$$

where Δ is the lag time and T is the total measurement time. In contrast to the ‘statistically averaged’ MSD, each TAMSD is an inherently random quantity (even for BM) [16, 19]. Therefore, averaging over N independent TAMSDs is often performed to compute the mean,

$$\langle \overline{\delta^2(\Delta)} \rangle = \frac{1}{N} \sum_{i=1}^N \overline{\delta_i^2(\Delta)}. \quad (4)$$

For a fixed lag time Δ , a stochastic process is called ergodic if its MSD and TAMSD are identical in the limit of long observation times [16, 19], i.e. when

$$\lim_{\Delta/T \rightarrow 0} \overline{\delta^2(\Delta)} = \langle x^2(\Delta) \rangle. \quad (5)$$

The randomness of each TAMSD realisation at a finite T gives rise to a certain amplitude scatter of $\overline{\delta_i^2(\Delta, T)}$ around the average (4). This scatter can be quantified by the EB parameter [16, 19, 39]

$$\text{EB}(\Delta) = \langle \xi^2(\Delta) \rangle - 1, \quad (6)$$

where $\xi(\Delta) = \overline{\delta^2(\Delta)} / \langle \overline{\delta^2(\Delta)} \rangle$. Similar to the TAMSD, the EB parameter is clearly also a function of the trajectory length, $\text{EB}(\Delta, T)$. Hereafter, however, we write EB as a function of its most relevant variable (often, the lag time Δ). For ergodic processes, EB approaches zero for long observation times T and the distribution of normalised TAMSDs [42, 43, 123, 124] (named below $\phi(\xi)$), approaches the Dirac δ -function in the asymptotic limit [16, 19, 44], $\phi(\xi) \rightarrow \delta(\xi - 1)$. In that limit, the results of all individual measurements coincide. For example, for paradigmatic BM (in the continuous-time limit) one gets [39, 117, 120]

$$\lim_{\Delta/T \rightarrow 0} \text{EB}_{\text{BM}}^{\text{cont}}(\Delta) = \frac{4\Delta}{3T}, \quad (7)$$

see also below. For nonergodic stochastic processes—such, e.g., as continuous-time random walks and heterogeneous diffusion processes—EB attains finite values at $\Delta/T \rightarrow 0$ [16, 19, 29, 47, 50]. We refer the reader to some examples of transiently nonergodic [43, 124] and non-Gaussian [70, 125] behaviour. Note also that the spectral content of single non-Brownian trajectories was recently investigated [22, 126, 127] and extended to random-diffusivity dynamics [128].

2.3. Main equations of the DD model

In what follows we employ the minimal DD model defined by the system of equations (following reference [87])

$$\begin{cases} \frac{dx(t)}{dt} = \sqrt{2D(t)}\zeta_H(t) \\ D(t) = y^2(t) \\ \frac{dy(t)}{dt} = -\frac{y(t)}{\tau} + \sigma\eta(t). \end{cases} \quad (8)$$

Here σ is a noise intensity, while $\zeta_H(t)$ and $\eta(t)$ is fractional Gaussian [38, 39] and white Gaussian [16, 19] noise, respectively. Both noises have zero means and correlation functions

$$\langle \zeta_H(t_1)\zeta_H(t_2) \rangle \simeq 2D_{2H}H(2H-1)|t_1-t_2|^{2H-2} \quad (9)$$

(for $t_1 \neq t_2$) and

$$\langle \eta(t_1)\eta(t_2) \rangle = \delta(t_1 - t_2). \quad (10)$$

Here D_{2H} is the generalised diffusion coefficient. Extending the minimal DD model [87, 88] the diffusivity $D(t)$ in (8) is set to be the square of the Ornstein-Uhlenbeck process [129] with the correlation time τ . This guarantees non-negative diffusivities, $D(t) = y^2(t)$. The physical units of some model parameters and quantities are: $[y] = [D^{1/2}] = [K^{1/2}] = m/s^H$, $[\sigma] = m/s^{H+1/2}$, $[\eta] = 1/\sqrt{s}$, $[\zeta_H(t)] = s^{H-1}$, and $[D_{2H}] = 1$. We note here that the approach combining the features of both the FBM and DD models is pioneered in [130] and further developed here and, to the best of our knowledge, it has not been considered in the literature before.

3. Main results: TAMSD and EB

3.1. Magnitude and distribution of the TAMSDs for the DD-FBM model

Here, we compute the mean TAMSD for the DD-FBM model for $H \in (0, 1)$ and check the MSD-TAMSD equivalence. To be able to use the stationarity of the DD model, the initial condition for $y(t)$ is chosen from the equilibrium distribution (see section 4.3 for nonequilibrium conditions). The mean TAMSD can be obtained via expanding (4) and calculating the position-correlation function (see appendix A for details),

$$\langle \overline{\delta^2(\Delta)} \rangle = 4 \int_0^\Delta (\Delta - s_{12})G(s_{12})ds_{12}, \quad (11)$$

where the velocity autocorrelation function of the DD model is

$$G(s_{12}) = \langle \sqrt{D(s_1)}\sqrt{D(s_2)} \rangle \langle \zeta_H(s_1)\zeta_H(s_2) \rangle \quad (12)$$

and

$$s_{12} = |s_1 - s_2|. \quad (13)$$

For $H = 1/2$ the TAMSD (11) reduces to

$$\langle \overline{\delta^2(\Delta)} \rangle = (\sigma^2\tau) \times \Delta = 2D_{\text{eff}}\Delta, \quad (14)$$

in agreement with the results of references [87, 88].

The MSD for the DD-FBM model is obtained via integrating (8) with initial condition $x(0) = 0$, yielding

$$\begin{aligned} \langle x^2(t) \rangle &= 2 \int_0^t ds_1 \int_0^t ds_2 \langle \sqrt{D(s_1)}\sqrt{D(s_2)} \rangle \langle \zeta_H(s_1)\zeta_H(s_2) \rangle \\ &= 4 \int_0^t (t - s_{12})G(s_{12})ds_{12}. \end{aligned} \quad (15)$$

From equations (11) and (15) follows that the MSD and mean TAMSD are identical in the entire range of (lag) times,

$$\langle \overline{\delta^2(\Delta)} \rangle = \langle x^2(\Delta) \rangle. \quad (16)$$

As the DD-FBM process is self-averaging at $T \rightarrow \infty$, the equivalence holds on the level of single TAMSD trajectories and the diffusion process is therefore ergodic.

These theoretical predictions and results of computer simulations for the MSD and TAMSD in the DD-FBM model are presented in figure 2 for three values of the Hurst exponent H . Expression (15) for the MSD states that for persistent fluctuations ($1 > H > 1/2$) both for short and long times one obtains

$$\langle x^2(t) \rangle \sim t^{2H}, \tag{17}$$

while for the antipersistent situation ($0 < H < 1/2$) a crossover from subdiffusive to Brownian behaviour is observed at long times, see figure 2. This behaviour observed in simulations is consistent with the analytical predictions stemming from the general MSD expression (15), as clarified in detail in reference [130].

Mathematically, repeating the arguments of reference [130], at short times ($s_{12} \ll \tau$) the diffusivity correlator

$$K(s_{12}) = \left\langle \sqrt{D(s_1)} \sqrt{D(s_2)} \right\rangle \tag{18}$$

in equation (15) approaches $(1/2)\sigma^2\tau$, see figure 7. This yields the anomalous MSD scaling

$$\langle x^2(t) \rangle \approx (D_{2H}/2)\sigma^2\tau \times t^{2H} \tag{19}$$

at short times, both for the persistent and antipersistent situations. At long times we have to separate persistent and antipersistent motion. In the persistent case, $1 > H > 1/2$, the leading contribution to the integral (15) at long times comes from large s_{12} , owing to a slow decay of the noise-autocorrelation function. We thus have a monotonically decreasing correlator (18) with the limit $K(s_{12} \gg \tau) \rightarrow (1/\pi)\sigma^2\tau$ (see figure 7) that yields *anomalous* MSD growth [130]

$$\langle x^2(t) \rangle = (2D_{2H}/\pi)\sigma^2\tau \times t^{2H}. \tag{20}$$

In the antipersistent case, via splitting the integral (15) we arrive at the leading MSD contribution $4t \int_0^\infty K(s_{12}) \langle \zeta_H(s_1) \zeta_H(s_2) \rangle ds_{12}$, where (due to convergence of the integrand) the upper limit was set to infinity, $t \rightarrow \infty$ [130]. This leading MSD term at long times yields the *linear* growth,

$$\langle x^2(t) \rangle \approx 2\bar{D}t, \tag{21}$$

with the effective diffusivity $\bar{D} = \lim_{\delta \rightarrow 0} 2 \int_0^{+\infty} K(s_{12}) \langle \zeta_H(s_1) \zeta_H(s_2) \rangle ds_{12}$ (where δ is the smoothing parameter of the correlation function [38, 130]). Here, the crossover time from the short-time law (19) to the long-time linear diffusion scaling laws (20) and (21) is always the correlation time τ , independent on the actual value of the Hurst exponent H .

Physically, the absence of the crossover and MSD scaling (19) in the entire range of times for persistent motion and the crossover from the short-time behaviour (19) to the long-time linear MSD behaviour (21) for antipersistent noise is owing to the fact that antipersistent motion for FBM delicately depends on the exact vanishing of the cumulative correlation, in contrast, e.g., to an analogous process with cut-off noise correlator [46].

Specifically, from our simulations at $\Delta \approx \tau$ and $H = 1/10$ this crossover is distinct both for

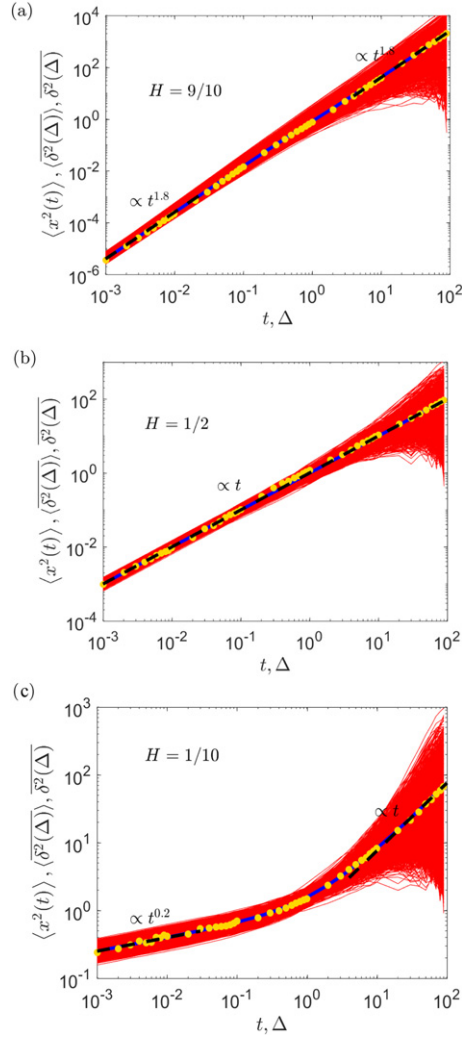


Figure 2. MSD (filled orange circles) and mean TAMSD (blue thick curves) as well as individual TAMSDs (red thin curves) for the DD-FBM model obtained from computer simulations for $H = 9/10$ (panel (a)), $1/2$ (b), and $1/10$ (c). The short-time MSD asymptote (19) and long-time scaling relations (20) and (21) are shown as the dashed lines. Parameters: the correlation time is $\tau = 1$, the noise intensity is $\sigma = 1$, the total trace length is $T = 10^2$, the integration time-step is $\delta t = 10^{-3}$, and the number of independent trajectories for averaging is $N = 10^3$. The same values of δt and N are used in all other plots. The values of the generalised diffusion coefficient in all our simulations and in the theoretical results shown above was fixed to $D_{2H} = 1/2$.

the MSD and mean TAMSD, see figure 2. We observe that the spread of individual TAMSDs for short lag times is larger for subdiffusion. From equation (A5) we also see that the mean TAMSD is independent of the total time T for all values of H . This is in contrast to ageing nonstationary processes [23, 116, 131, 132]. Note that experimentally short-time plateaus for the MSD and mean TAMSD can emerge due to localisation errors of particle positions [133,

134]. We also refer to the recent analysis of the effect of particle-localisation errors [135] on deviations of the short-time EB behaviour, above the BM asymptote (7).

3.2. Plateau values of EB

Here, we present the results for the EB parameter of the DD-FBM model in the limit of long traces, such that $T \gg \tau$. As for $H = 1/2$ the correlation function for fractional Gaussian noise, equation (9), reduces to the δ -function, we get exact analytical results for EB. For arbitrary $H \in (0, 1)$ the complicated correlation function (9) hampers an exact analytical expression for EB in the DD-FBM model and, thus, we resort to simulations.

3.2.1. Brownian case $H = 1/2$ for the DD-FBM model. The EB parameter of the DD-FBM model at $H = 1/2$ is calculated separately in the domains of lag times $0 < \Delta < T/2$ and $T/2 < \Delta < T$, similarly as in references [117, 120], and for long trajectories ($T \gg \tau$). For $0 < \Delta < T/2$ we get (see appendix B)

$$\begin{aligned} \text{EB}_{\text{DD+BM}}(\Delta) &= \frac{\left(\frac{4\Delta}{3} + 6\tau - \frac{4\tau^2}{\Delta} - \frac{2\tau^3}{\Delta^2} e^{-\frac{2\Delta}{\tau}} + \frac{2\tau^3}{\Delta^2}\right)}{(T-\Delta)} + \frac{\tau^4}{(T-\Delta)^2 \Delta^2} \\ &\times \left(\frac{3}{2} - \frac{3\Delta}{\tau} + \frac{2\Delta^2}{\tau^2} - \frac{2\Delta^3}{\tau^3} - \frac{\Delta^4}{3\tau^4} - \frac{3e^{-\frac{2\Delta}{\tau}}}{2} + \frac{e^{-\frac{2(T-2\Delta)}{\tau}}}{4} - \frac{e^{-\frac{2(T-\Delta)}{\tau}}}{2} + \frac{e^{-\frac{2T}{\tau}}}{4}\right). \end{aligned} \quad (22)$$

From equation (22), the leading order in $1/T$ yields

$$\text{EB}_{\text{DD+BM}}(\Delta) \sim \frac{4\Delta}{3T} + \frac{6\tau}{T} - \frac{4\tau^2}{\Delta T} - \frac{2\tau^3 e^{-\frac{2\Delta}{\tau}}}{\Delta^2 T} + \frac{2\tau^3}{\Delta^2 T} \quad (23)$$

and we get the respective asymptotes as

$$\text{EB}_{\text{DD+BM}}(\Delta) \approx \begin{cases} 2\tau/T, & \Delta \ll \tau \\ 4\Delta/(3T), & \Delta \gg \tau \end{cases}. \quad (24)$$

We thus find that the standard result for BM [117, 120] is reached at $\Delta \gg \tau$, while a remarkable plateau is reached for $\text{EB}_{\text{DD+BM}}(\Delta)$ at short lag times. As follows from (22) and (24), the correlation time τ emerges as the fundamental time-scale that controls the crossover behaviour of $\text{EB}_{\text{DD+BM}}(\Delta)$.

For $T/2 < \Delta < T$ the EB parameter is (see appendix B)

$$\begin{aligned} \text{EB}_{\text{DD+BM}}(\Delta) &= \frac{T^2 - 6T\Delta - 6T\tau + 11\Delta^2 + 24\Delta\tau - 6\tau^2}{3\Delta^2} \\ &- \frac{\tau^3 (1 + 2e^{-2\Delta/\tau})}{(T-\Delta)\Delta^2} + \frac{\tau^4 \left(2 - 2e^{-\frac{2(T-\Delta)}{\tau}} + 5e^{-\frac{2(T-2\Delta)}{\tau}} + e^{-\frac{2T}{\tau}} - 6e^{-\frac{2\Delta}{\tau}}\right)}{4(T-\Delta)^2 \Delta^2}. \end{aligned} \quad (25)$$

For long enough T the first term in expression (25) gives

$$\text{EB}_{\text{DD+BM}}(\Delta) \sim \frac{T^2/3 - 2T\Delta - 2T\tau + 11\Delta^2/3 + 8\Delta\tau - 2\tau^2}{\Delta^2}. \quad (26)$$

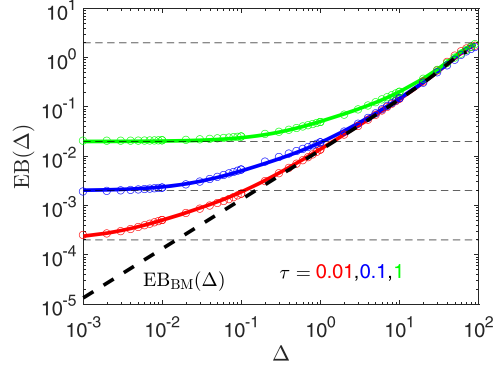


Figure 3. Analytical (solid coloured curves) and numerical (coloured circles) results for the EB parameter of the DD-FBM model for $H = 1/2$. The thick black dashed line is the continuous-time analytical result for EB of BM, equation (7). The terminal value of $EB(\Delta = T) = 2$ is the thin dashed line. Parameters: $H = 1/2$, $\sigma = 1$, $T = 10^2$.

At $\tau \ll \Delta$ and $\tau \ll (T - \Delta)$ this expression yields

$$EB_{DD+BM}(\Delta) \sim \frac{11(\Delta/T)^2 - 6(\Delta/T) + 1}{3(\Delta/T)^2}, \quad (27)$$

similar to EB of standard BM [117, 120]. Towards the end of the trajectories, at $\Delta \rightarrow T$, the value

$$EB = 2 \quad (28)$$

is reached and from equation (27) one gets the first-order correction to this value as

$$EB_{DD+BM}(\Delta) \approx 2 - 4(T - \Delta)/(3T). \quad (29)$$

We note that equations (27) and (29) also hold for BM in the respective range of lag times [117].

In figure 3 the analytical and numerical results for the EB parameter of the DD-FBM model at $H = 1/2$ are presented. For the case $\tau \ll T$, $EB_{DD+BM}(\Delta)$ starts from the plateau value $2\tau/T$ (thin dashed lines in the plot, equation (24)) at short enough lag times, $\Delta \ll \tau$. The BM EB asymptote (7) is approached for $\Delta \gg \tau$, as equation (24) predicts. In figure 3 the results for varying correlation times are plotted. We find that, as for longer τ the EB plateau value increases (see equation (24)) and the region of lag times where $EB_{DD+FBM}(\Delta)$ stays nearly constant becomes more extended. Concurrently, for larger τ values the region of lag times where $EB_{DD+BM}(\Delta)$ follows the BM law (7) shifts towards larger Δ values, see the curve for $\tau = 1$ in figure 3.

3.2.2. General case of $H \in (0, 1)$ for ordinary FBM: discreteness effects. We start by discussing the ergodic properties of free (unconstrained) ordinary or standard FBM. The expression for $EB_{FBM}(\Delta)$ at short lag times $\Delta/T \ll 1$ was derived analytically in reference [39] in the continuous-time representation, namely

$$EB_{FBM}^{\text{cont}}(\Delta) \sim \begin{cases} C_1 \times (\Delta/T)^1, & 0 < H < 3/4 \\ C_2 \times (\Delta/T)^{4-4H}, & 1 > H > 3/4 \end{cases}, \quad (30)$$

where the coefficients are

$$C_1(H) = \int_0^\infty [(1+s)^{2H} + |1-s|^{2H} - 2s^{2H}]^2 ds \tag{31}$$

and

$$C_2(H) = [2H(2H-1)]^2 \left(\frac{1}{4H-3} - \frac{1}{4H-2} \right). \tag{32}$$

The variation of $C_1(H)$ is presented in figure 8. The main conclusion is that for short lag times $EB_{\text{FBM}}^{\text{cont}}(\Delta)$ scales linearly with Δ/T for $H < 3/4$, while the scaling of $EB(\Delta/T)$ is sublinear for $1 > H > 3/4$ ($H = 3/4$ is a ‘critical point’ [39, 44], see figure 5 below and the detailed behaviour in figure 9). In other words, the degree of reproducibility of individual TAMSD realisations increases linearly with the trace length for $H < 3/4$ and the statistical uncertainties decrease slower than linearly with T in the range of Hurst exponents $1 > H > 3/4$ (it was erroneously predicted in reference [39] to diverge at $H = 3/4$, see below). The canonical continuous-time result for free BM, equation (7), follows from equation (30) at $H = 1/2$.

In the continuous-time formulation, the original EB results for FBM [39] were recently reexamined [44]. Specifically, within a more rigorous analytical framework for $EB_{\text{FBM}}(\Delta)$ it was revealed that the ‘critical point’ at $H = 3/4$ disappears and the behaviour of EB is, in fact, *continuous* as function of H across this point, see figure 1 in reference [44]. This continuity agrees with the results of our FBM simulations presented in figure 5. Moreover, some unexpected results from computer simulations of FBM regarding the longer-tailed, non-Gaussian distributions $\phi(\xi)$ of individual TAMSDs—in particular, for progressively superdiffusive FBM and at longer lag times—were reported in figure 3 of reference [44].

The analytical predictions and the results of our computer simulations of FBM for $EB_{\text{FBM}}(\Delta)$ are shown in figure 4. We find that for $H > 3/4$ the continuous-time theory [39] and our computer simulations coincide in a large range of the lag times studied. However, due to the innate limitations of the short-lag-time EB expansion (30), towards the end of the trajectory the simulations yield $EB \rightarrow 2$ (28), while the (extrapolated) continuous-time prediction [39] would give $EB(\Delta \rightarrow T) \approx C_2(H)$, as follows from equation (32).

In contrast, for $H < 3/4$ at short lag times a plateau-like, saturation behaviour of EB is found, while the continuous-time theory [39] predicts a linear scaling with (Δ/T) , see equation (30). This is the vital effect of a finite time-step used in computer simulations, δt . The region of EB saturation with Δ is particularly pronounced for small Hurst exponents, at which the EB plateau can occupy a considerable range of lag times (see, e.g., the curve for $H = 1/100$ in figure 4 and also the results of figure 10).

From the general discrete-time expression (C4) for $EB_{\text{FBM}}^{\text{disc}}(\Delta)$ we find that at $\Delta_1 = \delta t$ and $H = 1/2$ the residual value

$$EB_{\text{BM}}^{\text{disc}}(\Delta_1) \sim 2/(N-1) \tag{33}$$

is approached, while for $H \rightarrow 0$ one gets (see also reference [137])

$$EB_{\text{FBM}}^{\text{disc}}(\Delta_1) \sim \frac{2}{N-1} \left(\frac{3}{2} - \frac{1}{2(N-1)} \right). \tag{34}$$

Here $N = T/\delta t$ is the number of elementary time-intervals in the trajectory. In the region

$$0 < H \lesssim 1/2 \tag{35}$$

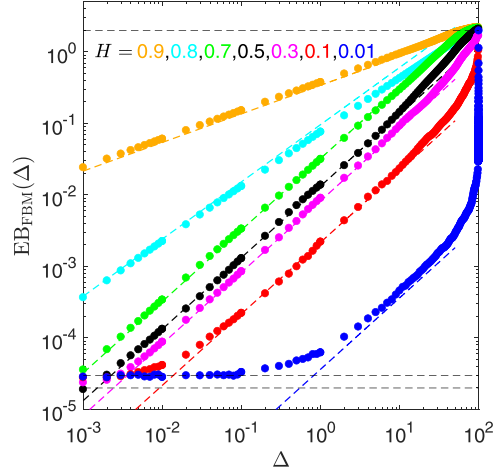


Figure 4. Analytical predictions of the continuous-time theory [39] (dashed coloured lines, equation (30)) and results of computer simulations (coloured circles) for the EB parameter of free ordinary FBM. The thin dashed lines indicate the residual EB values (33) and (34) as well as the terminal value $EB = 2$ reached at $\Delta \rightarrow T$. Parameters: $T = 10^2$, $\delta t = 10^{-3}$, $D_{2H} = 1/2$.

we get the approximate, rather weak variation of the residual EB value with H (see appendix C),

$$EB_{\text{FBM}}^{\text{disc}}(\Delta_1) \sim \frac{2}{N-1} + \frac{(N-2)(2^{2H}-2)^2}{(N-1)^2}. \quad (36)$$

Note that (33) follows from this expression at $H = 1/2$. The lag time up to which this saturating EB behaviour is detected can be estimated as

$$\Delta_{\text{pl}}^{\text{disc}}(H) \sim 2 \times \delta t / C_1(H), \quad (37)$$

(see appendix C and figure 10 for details), where $C_1(H)$ is given by equation (31). In the range

$$1 > H > 3/4 \quad (38)$$

from equation (C4) we get (in the leading order)

$$EB_{\text{FBM}}^{\text{disc}}(\Delta_1) \sim C_2(H)/(N-1)^{4-4H}, \quad (39)$$

that is identical to the result of continuous-time theory [39], see equation (30).

In figure 4 we plot the result for $EB_{\text{FBM}}(\Delta)$ starting from the shortest lag time, $\Delta_1 = \delta t$. For $H > 3/4$ the results for EB from computer simulations are in full agreement with the predictions of the continuous-time theory (30) and the discrete-time framework (39) for all lag times. At the end of the trajectories EB approaches the expected value $EB = 2$ (see equation (C7)). At short lag times $EB_{\text{FBM}}(\Delta)$ in the discrete-time framework features a plateau for $0 < H < H_{\text{pl}} \approx 0.64$ (as given by equation (C12)), as follows from the theoretical estimations (C9) and (C10). This plateau trend is most pronounced for the smallest Hurst exponents, extending towards longer lag times (as figure 10 explicitly quantifies). All these features are also consistent with the results of computer simulations, as illustrated in figure 4 for the

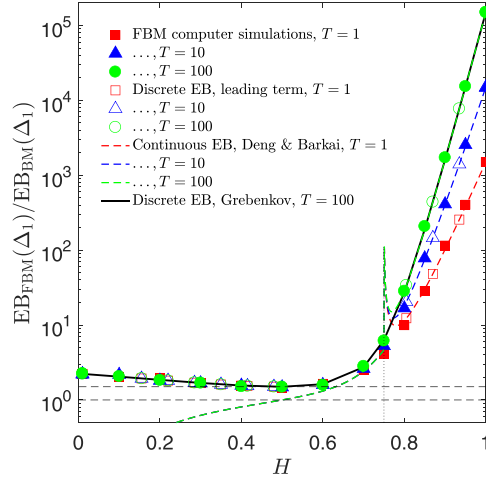


Figure 5. $EB_{\text{FBM}}(\Delta)$ normalised to the BM behaviour $EB_{\text{BM}}^{\text{cont}}(\Delta)$ (equation (7)) plotted versus the Hurst exponent H at the shortest lag time $\Delta_1 \equiv \delta t = 10^{-3}$. The results of our computer simulations are the filled symbols. The analytical results of the continuous-time theory [39], see equation (30), are the dashed coloured curves. The results of the discrete-time EB-derivation scheme—see equation (C4) and also reference [137]—is the solid black curve (shown for $T = 10^2$ only, not to cover the dashed coloured curves of reference [39] for $H > 1/2$). The thin dashed black lines are the discreteness-induced plateaus, equations (33) and (34). The thin vertical dotted line indicates the ‘critical point’ of the continuous-time EB theory for FBM [39]. The behaviour of EB near $H = 3/4$ is detailed in figure 9. Parameters: $T = 10^0, 10^1, 10^2$ for the respective colours, $D_{2H} = 1/2$.

time-step $\delta t = 10^{-3}$ and in figure 11 for $\delta t = 10^{-6}$. Note, however, that for a nearly ballistic Hurst exponent, at $H = 0.99$, in the region of extremely small lag times a rapid and unexpected reduction of EB for FBM is observed. This effect requires additional future consideration.

The results of computer simulations and the discrete-time-induced EB plateau (33) at Δ_1 are superimposing in the region $0 < H \lesssim 1/2$, see figure 5. The predictions of the continuous-time theory [39] deviate from the results of computer simulations in the range $0 < H \lesssim 1/2$, and, most pronouncedly, for very small values of the Hurst exponent.

In the region $0 < H < 3/4$ the continuous-time $EB(\Delta)$ results for BM and FBM are linear in Δ/T , see equation (30). This linearity yields the universal, T -independent behaviour for the normalised quantity $EB_{\text{FBM}}^{\text{cont}}(\Delta)/EB_{\text{BM}}^{\text{cont}}(\Delta)$ at short lag times in this region of H exponents, see the coloured dashed curves in figure 5. On the contrary, because of the sublinear scaling of $EB_{\text{FBM}}^{\text{cont}}(\Delta)$ with Δ/T in the region $3/4 < H < 1$ the predictions for the ratio $EB_{\text{FBM}}^{\text{cont}}(\Delta)/EB_{\text{BM}}^{\text{cont}}(\Delta)$ split up as T is being varied, see figure 5.

We also find that the H -dependent residual values of the rescaled EB parameter, $EB_{\text{FBM}}(\Delta_1)/EB_{\text{BM}}^{\text{cont}}(\Delta_1)$, at $0 < H \lesssim 1/2$, equation (36), are nearly independent on the trajectory length T , while in the range of Hurst exponents $1/2 \lesssim H < 1$ the ratio $EB_{\text{FBM}}(\Delta_1)/EB_{\text{BM}}^{\text{cont}}(\Delta_1)$ is highly sensitive to T . The values of the ratio $EB_{\text{FBM}}(\Delta_1)/EB_{\text{BM}}^{\text{cont}}(\Delta_1)$ decisively split up for different trajectory lengths in the range $1 > H \gtrsim 1/2$, as demonstrated in figures 5 and 9. As all $EB_{\text{FBM}}(\Delta_1)$ data in figure 5 are renormalised to the continuous-time classical result for the EB parameter of BM, $EB_{\text{BM}}^{\text{cont}}(\Delta_1)$, at $H = 1/2$ we find that the result of the discrete-time theory is a factor of $3/2$ higher than that of the continuous-time EB

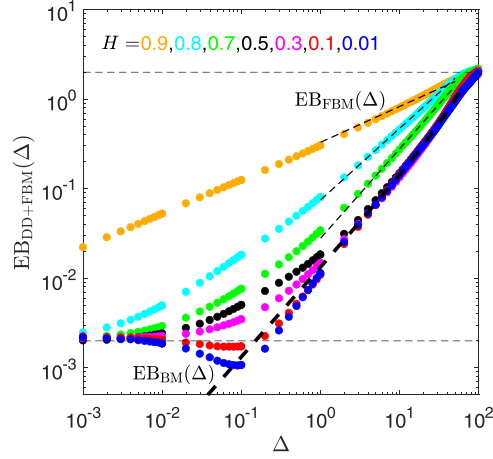


Figure 6. EB parameter of the DD-FBM model as obtained from computer simulations for varying Hurst exponents (the values are indicated in the plot). The result for BM, equation (7), is shown as the thick dashed line. The plateau value (40) and the limiting value of EB = 2 at $\Delta \rightarrow T$ are the thin dashed lines. The asymptotes of FBM at long lag times, equation (30), are the dashed lines at long lag times. Parameters: $\tau = 0.1$, $\sigma = 1$, $T = 10^2$, $D_{2H} = 1/2$, and $N = 10^3$.

calculation, while at $H = 0$ the EB value in the discrete model $EB_{FBM}^{disc}(\Delta_1)$ is a factor $(3/2)^2$ larger than $EB_{BM}^{cont}(\Delta_1)$ (see equations (7), (33) and (34)).

Physically, the nonmonotonicity of the rescaled EB parameter $EB_{FBM}(\Delta_1)/EB_{BM}^{cont}(\Delta_1)$ as a function of H presented in figure 4 is owing to the fact that for pure BM (at $H = 1/2$) the EB parameter attains the smallest value (natural for the most ergodic situation). The system becomes slightly less ergodic as H decreases from $H = 1/2$ towards $H = 0$ and the deviations from ergodicity turn much more dramatic as the Hurst exponent grows in the opposite direction from $H = 1/2$ towards $H = 1$ (the ultimate ballistic regime). This physically intuitive behaviour is consistent with all relevant limits clarified in figure 4, both within the continuous-time [39] and discrete-time (reference [137] and the current study) approaches. The overall dependence of $EB_{FBM}(\Delta_1)/EB_{BM}^{cont}(\Delta_1)$ for FBM—for the results of continuous-time theory, the discrete-time analytical theory, and the innately discretised computer simulations—as a function of exponent H (see figure 4) as well as the universality of the ratio $EB_{FBM}^{disc}(\Delta_1)/EB_{BM}^{cont}(\Delta_1)$ for varying trajectory lengths in the region $0 < H \lesssim 1/2$ (see figure 5) are similar to those trends we observed for another Gaussian anomalous-diffusion process, namely so-called scaled BM (e.g., see figure 3(a) of our recent study [136]).

After the current study was finished, we became aware of reference [137] presenting detailed calculations of EB in the discrete-time scheme both for standard BM as well as for FBM. In figure 5 we show that the analytical results of equation (37) in reference [137]—which are identical to our EB derivation in equation (C4)—agree excellently with the results of our computer simulations. Note also that the emergence of the residual EB value for the discrete-time simulations was already presented (but not rationalised) in figure 6 of the original study [39].

3.2.3. General case $H \in (0, 1)$ for the DD-FBM model. We now consider the situation of FBM-driven DD motion. We present results from computer simulations for $EB_{DD+FBM}(\Delta)$ at different H in figure 6 and compare them to the results for $EB_{FBM}(\Delta)$ obtained in figure 4. For

short lag times ($\Delta \ll \tau$) and for all values of H , EB is found to approach a plateau (subscript ‘pl’) with the residual value

$$EB_{\text{pl,DD+FBM}} \approx 2\tau/T. \quad (40)$$

In figure 12 we check this functional form via examining the plateau values for varying correlation time τ . The magnitude of EB at $\Delta \ll \tau$ approaches the plateau (33) (thin dashed line in figure 6) and it shows the FBM-like asymptotic law (30) at long lag times $\Delta \gg \tau$ (thick dashed lines in figure 6). As figures 6 and 12 show, EB for larger H approaches this plateau at progressively shorter lag times. This trend is similar to that of $\Delta_{\text{pl}}^{\text{disc}}$ for the discreteness-induced EB plateau for pure FBM, shown in figure 10. Performing computer simulations at varying correlation times τ for the relatively large Hurst exponent $H = 9/10$ we confirmed the universal EB plateau within the DD-FBM model, see figure 13, which is realised also (at even shorter lag times) for $H = 9/10$ in figure 6. The EB plateau for the DD-FBM model is reached at shorter lag times also for larger Hurst exponents. To make this region visible, in figure 14 we present results of simulations for shorter trajectories and shorter elementary lag-time-step used in simulations.

We observe three clear differences between the FBM and DD-FBM models. (i) At short lag times, in the DD-FBM model the DD-induced EB plateau (40) is different from the discreteness-induced residual value (33) for FBM. Moreover, while equation (40) is valid for all H , the EB of FBM approaches the plateau at $H \lesssim 1/2$ only. (ii) For lag times $\Delta \simeq \tau$ and small H values (see the results for $H = 1/100$ in figure 15), $EB_{\text{DD+FBM}}(\Delta)$ grows nonmonotonically in Δ and shows a minimum at $\Delta \approx \tau$. We quantify the position of this minimum in figure 15, also verifying the width of the distributions of individual TAMSDs in figure 16. Near this minimum, at intermediate lag times, $EB_{\text{DD+FBM}}(\Delta)$ also features a drop below the paradigmatic BM asymptote (7). (iii) For long lag times, $\Delta \gg \tau$, $EB_{\text{DD+FBM}}(\Delta)$ at $H < 1/2$ approaches the continuous BM result, while for $1/2 < H < 1$ the FBM limit for the EB parameter (equation (30)) is obtained, see figure 6.

To quantify inaccuracies of the numerical computation of the means $\langle \overline{\delta^2(\Delta)} \rangle$ and $\langle (\overline{\delta^2(\Delta)})^2 \rangle$, in figure 17 we present the respective error bars versus lag time for the computations within the DD-FBM model. We find that, as expected, the error bars grow in magnitude at later lag times, due to worsening statistics of averaging. In the plateau-like region of $EB_{\text{DD+FBM}}(\Delta)$ versus H , however, the error bars are small enough for us to be confident in the existence of the plateau region itself and of the dip in $EB_{\text{DD+FBM}}(\Delta)$ at $\Delta \sim \tau$ for very small H values (see figure 6). These features are not artefacts of poor averaging. Moreover, the magnitude of the error bars increases for larger exponents H , in agreement with equation (39).

4. Discussion and conclusions

4.1. Summary of the main results

We considered the combination of DD dynamics [67, 87] and canonical FBM. Our main focus was to quantify the TAMSD fluctuations naturally occurring in experiments and gauged by the EB parameter. In particular, we analysed the plateau-like residual EB behaviour. Specifically, assuming the stationarity of the diffusivity distribution, the MSD and TAMSD of the DD-FBM model were studied. We found that the MSD and mean TAMSD are equal for both normal and anomalous diffusion in the entire range of (lag) times. For $H < 1/2$ we described a crossover

in the TAMSD from subdiffusion to normal diffusion at lag times of the order of the DD correlation time τ , figure 2. From this TAMSD behaviour, the correlation time of heterogeneous environments featuring DD properties can potentially be extracted for SPT data sets.

We revealed an intricate nonergodic behaviour in this DD-FBM model. Specifically, considering long trajectories with $T \gg \tau$, a crossover behaviour was found: for short lag times, $\Delta \ll \tau$, the EB parameter was shown to approach a plateau with a residual value $EB_{\text{pl,DD+FBM}} \sim 2(\tau/T)$, which scales linearly with the ratio of the DD correlation time τ and the total measurement time T . Conversely, for long lag times $\Delta \gg \tau$, $EB_{\text{DD+FBM}}(\Delta)$ behaved the same way as for ordinary or standard FBM, see figure 6. The residual value of $EB_{\text{DD+FBM}}(\Delta)$ was shown to be universal for all values of the Hurst exponents H .

Moreover, we demonstrated that for small values of H the variation of $EB_{\text{DD+FBM}}(\Delta)$ was nonmonotonic, featuring a clear systematic minimum at $\Delta \approx \tau$, see figure 6. Towards the end of the trajectories, at $\Delta \rightarrow T$, we found the expected value $EB = 2$. When simulating standard FBM, we found a plateau-like behaviour for $EB_{\text{FBM}}(\Delta)$ at $H \lesssim 1/2$ that scaled as the ratio of the time-step to the total trace length and depended weakly on the Hurst exponent, see figure 4. The plateau-like behaviour of $EB_{\text{pl,DD+FBM}}$ and $EB_{\text{pl,FBM}}^{\text{disc}}$ (both analytically and via computer simulations) is the key result of the current study. The correlation time τ in the DD and DD-FBM models is, therefore, a fundamental time-scale for the ergodic behaviour, similar to the single time-step in the free discrete-time dynamics.

4.2. Other DD-related models

The relative standard deviation of fluctuations of individual TAMSDs (\sqrt{EB} in our notations) was rationalised for a model of the Langevin equation with time-dependent and fluctuating diffusivity in reference [80]. This model of multiplicatively coupled Langevin equations enables one to assess EB via studying the relaxation behaviour of the noise-coefficient matrix (or the matrix of instantaneous diffusion coefficients). In this approach the process $\mathbf{B}(t) = \sqrt{2D(t)} \times \mathbf{1}$ in the (multidimensional) Langevin equation

$$d\mathbf{r}/dt = \sqrt{2D(t)} \times \mathbf{w}(t) \tag{41}$$

was assumed to be ergodic. The general expression for EB was derived [80] in the continuous limit for arbitrary two-time-point correlation functions of the diffusivity matrix. For the one-dimensional case, in the limit of long observation times and short lag times—and, additionally, when the relaxation time of the diffusivity (denoted below τ_1) is much longer than the lag time, the diffusivity relaxation function $\psi_1(t)$ decays fast enough, and the relaxation time is much shorter than the trajectory length (i.e., when $\tau_1 \gg \Delta$ and $\tau_1 \ll T$)—the approximate EB expression was derived as (see equation (33) in reference [80])

$$EB(\Delta) \approx \frac{2}{T} \int_0^\infty \psi_1(s) ds. \tag{42}$$

For the simplest (and most common) situation of exponential relaxation, $\psi_1(t) = \psi_1(0)e^{-t/\tau_1} \propto e^{-t/\tau_1}$, from (42) it follows that when the lag time is the shortest time-scale in the problem EB saturates at

$$EB(\Delta_1) \approx 2\tau_1/T. \tag{43}$$

This value is identical to our predictions for the EB plateau in the DD-FBM model, equation (40).

As derived in reference [80], for the (Markovian) two-state diffusion model—the Kärger model [138] (see also references [139, 140] for its recent applications)—with the diffusion coefficients D_1 and $D_2 > D_1$ a dependence similar to equation (43) can be obtained for the EB parameter in reference [80]. Namely, for the transition rates from the state with diffusivity D_1 to the state with D_2 being k_{12} (and vice versa for k_{21}), the equilibrium probabilities of the respective diffusion states are $p_1 = k_{21}/(k_{12} + k_{21})$ and $p_2 = k_{12}/(k_{12} + k_{21})$. The characteristic relaxation time is

$$\tau_{1,2} = 1/(k_{12} + k_{21}) \quad (44)$$

and in the same limit (at $\tau_{1,2} \gg \Delta$ and $\tau_{1,2} \ll T$) EB has the same functional dependence on $\tau_{1,2}/T$, that is [80]

$$\text{EB}(\Delta_1) \approx \psi_1(0) \times 2\tau_{1,2}/T, \quad (45)$$

where $\psi_1(0) = p_1 p_2 (D_2 - D_1)^2 / (p_1 D_1 + p_2 D_2)^2$ (see equation (57) in reference [80]). These results were also confirmed by computer simulations in reference [80]. The generalisation of these EB calculations for such a dichotomic stochastic-diffusivity model for the situation when switching between the diffusion states is governed by a power-law distribution was developed in the same group [81, 82, 84].

The short-lag-time plateau of EB appears to be *universal* for the models of diffusing or fluctuating diffusivity, also in the presence of *anomalous* underlying dynamics, as we demonstrated above for the DD-FBM model. The model of temporally fluctuating diffusivity has recently been applied by the same group to rationalise the dynamic interactions between membrane-binding proteins and lipids in model biomembranes [104]. Finally, we refer the reader also to the discussion of short measurement times and ‘apparent’ ergodicity breaking for the two-state switching diffusion, recently presented in reference [98].

4.3. Effects of nonequilibrium initial conditions

Finally, the TAMSD and EB results obtained and discussed above involve the stationarity of the DD distribution. Nonequilibrium conditions can, however, also be relevant. For instance, recently the MSD of the DD model of normal diffusion with initial condition $D(0) = 0$ was discussed [88]. The MSD was demonstrated to be ballistic for $t \ll \tau$ and linear for long times [88]. We found in the model (8) that the mean TAMSD for the initial condition $D(0) = y(0)^2 = 0$ and for $H = 1/2$ follows

$$\langle \overline{\delta^2(\Delta)} \rangle = \sigma^2 \tau \Delta + \frac{\sigma^2 \tau^3 (e^{-2(T-\Delta)/\tau} - e^{-2T/\tau} + e^{-2\Delta/\tau} - 1)}{4(T - \Delta)}, \quad (46)$$

see figure 18. This expression converges to equation (14) as $T \rightarrow \infty$ that is physically clear: the long measurement time eliminates effects of initial conditions in this system. The nonequilibrium initial DD conditions have no effect on EB, also in the general case $H \in (0, 1)$.

4.4. Conclusions

Concluding, we here highlighted the role of the correlation time in the stochastic dynamics with random diffusivities. Similar to a finite elementary time-step in discrete-time diffusion models of free, unconstrained motion (BM, FBM), the correlation time represents the fundamental time-scale in the random-diffusivity dynamics: for lag times shorter than this correlation time

the fluctuations of the TAMSDs reach a finite asymptotic spread, i.e., a finite residual value of the ergodicity breaking parameter EB. This effect is expected to be relevant for modern high-resolution single-particle-tracking experiments, to be considered in the data analysis. It will be interesting to analyse whether nonergodic anomalous-diffusion processes will exhibit similar features.

Acknowledgments

WW is supported by the Chinese Council Scholarship (Grant No. 201806830031). ST acknowledges Deutscher Akademischer Austauschdienst (DAAD) for a PhD Scholarship (Programme ID 57214224). XL and WW acknowledge financial support from the National Natural Science Foundation of China (NNSFC, Grants 11472126 and 11232007) and the Priority Academic Programme Development of Jiangsu Higher Education Institutions (PAPD). RM and AVC acknowledge financial support by Deutsche Forschungsgemeinschaft (DFG Grant ME 1535/7-1). RM also acknowledges the Foundation for Polish Science (Fundacja na rzecz Nauki Polskiej) for support within an Alexander von Humboldt Polish Honorary Research Scholarship. FS acknowledges financial support of the Department of Physics and Astronomy of Padua University (191017 BIRD-PRD project).

Abbreviations

SPT	Single-particle tracking
MSD	Mean-squared displacement
TAMSD	Time-averaged MSD
PDF	Probability density function
DD model	Diffusing-diffusivity model
BM	Brownian motion
FBM	Fractional Brownian motion

Appendix A. TAMSD of the DD-FBM model

Here, we present the details of the TAMSD calculations for the DD-FBM model, applicable for all values of the Hurst exponent H . Starting from the TAMSD definition (3),

$$\langle \overline{\delta^2(\Delta)} \rangle = \frac{\int_0^{T-\Delta} [\langle x^2(t+\Delta) \rangle + \langle x^2(t) \rangle - 2 \langle x(t+\Delta)x(t) \rangle] dt}{T-\Delta}, \quad (\text{A1})$$

and using the MSD (15), we have

$$\langle x^2(t+\Delta) \rangle = 4 \int_0^{t+\Delta} (t+\Delta-s_{12}) G(s_{12}) ds_{12}. \quad (\text{A2})$$

Next, we compute the position autocorrelation function with

$$s_{12} = |s_1 - s_2| \quad (\text{A3})$$

and $G(s_{12})$ defined in equation (12) as

$$\begin{aligned} \langle x(t + \Delta)x(t) \rangle &= 2 \int_0^{t+\Delta} ds_1 \int_0^t ds_2 G(|s_1 - s_2|) = 2 \int_0^t (t - s_{12})G(s_{12})ds_{12} \\ &\quad + 2 \int_0^{t+\Delta} (t - s_{12})G(s_{12})ds_{12} + 2 \int_0^\Delta s_{12}G(s_{12})ds_{12} + 2 \int_\Delta^{t+\Delta} \Delta G(s_{12})ds_{12}. \end{aligned} \tag{A4}$$

Substituting (A4) into (A1) we get equation (15), namely

$$\begin{aligned} \langle \overline{\delta^2(\Delta)} \rangle &= \frac{4}{T - \Delta} \int_0^{T-\Delta} \left[\int_0^\Delta (\Delta - s_{12})G(s_{12})ds_{12} \right] dt \\ &= 4 \int_0^\Delta (\Delta - s_{12})G(s_{12})ds_{12} = \langle x^2(\Delta) \rangle. \end{aligned} \tag{A5}$$

Appendix B. EB for the DD-FBM model at $H=1/2$

For $H = 1/2$ the ‘second moment’ of the TAMSD (after splitting the integrals into two parts),

$$\begin{aligned} \langle \left(\overline{\delta^2(\Delta)} \right)^2 \rangle &= \frac{1}{(T - \Delta)^2} \int_0^{T-\Delta} dt_1 \int_0^{T-\Delta} dt_2 \langle (x(t_1 + \Delta) - x(t_1))^2 (x(t_2 + \Delta) - x(t_2))^2 \rangle \\ &= \frac{2}{(T - \Delta)^2} \int_0^{T-\Delta} dt_1 \int_0^{t_1} dt_2 \langle (x(t_1 + \Delta) - x(t_1))^2 (x(t_2 + \Delta) - x(t_2))^2 \rangle, \end{aligned} \tag{B1}$$

is the most challenging quantity to compute. Using the Isserlis–Wick theorem for Gaussian processes with zero mean,

$$\begin{aligned} \langle x(t_1)x(t_2)x(t_3)x(t_4) \rangle &= \langle x(t_1)x(t_2) \rangle \langle x(t_3)x(t_4) \rangle \\ &\quad + \langle x(t_1)x(t_3) \rangle \langle x(t_2)x(t_4) \rangle + \langle x(t_1)x(t_4) \rangle \langle x(t_2)x(t_3) \rangle, \end{aligned} \tag{B2}$$

we expand all higher-order correlators via the pair correlators to get

$$\begin{aligned} &\langle (x(t_1 + \Delta) - x(t_1))^2 (x(t_2 + \Delta) - x(t_2))^2 \rangle \\ &= \begin{cases} 4A_1(t_1, t_2), & t_2 \leq t_1 - \Delta \\ 4(A_1(t_1, t_2) + 2A_2(t_1, t_2)), & t_2 \geq t_1 - \Delta \end{cases} \end{aligned} \tag{B3}$$

where

$$A_1(t_1, t_2) = \int_{t_1}^{t_1+\Delta} ds_1 \int_{t_2}^{t_2+\Delta} ds_2 \langle D(s_1)D(s_2) \rangle, \tag{B4}$$

$$A_2(t_1, t_2) = \int_{t_1}^{t_1+\Delta} ds_1 \int_{t_1}^{t_2+\Delta} ds_2 \langle D(s_1)D(s_2) \rangle, \tag{B5}$$

$$\langle D(s_1)D(s_2) \rangle = \frac{\sigma^4 \tau^2}{4} \left(1 + 2e^{-2|s_1 - s_2|/\tau} \right). \tag{B6}$$

To evaluate the integral (B1), we split the consideration into two cases, $0 < \Delta < T/2$ and $T > \Delta > T/2$, that yields

$$\begin{aligned} \left\langle \left(\overline{\delta^2(\Delta)} \right)^2 \right\rangle_{0 < \Delta < T/2} &= \frac{8}{(T - \Delta)^2} \left[\int_{\Delta}^{T-\Delta} dt_1 \int_0^{t_1-\Delta} dt_2 A_1(t_1, t_2) \right. \\ &+ \left. \int_0^{\Delta} dt_1 \int_0^{t_1} dt_2 (A_1(t_1, t_2) + 2A_2(t_1, t_2)) + \int_{\Delta}^{T-\Delta} dt_1 \int_{t_1-\Delta}^{t_1} dt_2 (A_1(t_1, t_2) + 2A_2(t_1, t_2)) \right] \end{aligned} \tag{B7}$$

and

$$\left\langle \left(\overline{\delta^2(\Delta)} \right)^2 \right\rangle_{T > \Delta > T/2} = \frac{8}{(T - \Delta)^2} \int_0^{T-\Delta} dt_1 \int_0^{t_1} dt_2 (A_1(t_1, t_2) + 2A_2(t_1, t_2)). \tag{B8}$$

Combining equations (B4), (B7) and (B8) with equation (6), we straightforwardly obtain the EB expressions of equations (23) and (25) in the main text.

Appendix C. EB for ordinary FBM

Here, we analyse the discrepancy between the theory and simulations of the EB parameter for FBM at short lag times, $\Delta \ll T$, arising from a discrete-time scheme employed in our simulations. Specifically, the TAMSD at the discrete points

$$\Delta_n = n \times \delta t \tag{C1}$$

is

$$\begin{aligned} \left\langle \left(\overline{\delta^2(\Delta_n)} \right)^2 \right\rangle &= \frac{\delta t^2}{(T - n \times \delta t)^2} \left\langle \sum_{i=1}^{T/\delta t - n} (x(t_i + n \times \delta t) - x(t_i))^2 \right. \\ &\times \left. \sum_{j=1}^{T/\delta t - n} (x(t_j + n \times \delta t) - x(t_j))^2 \right\rangle. \end{aligned} \tag{C2}$$

Using the Isserlis–Wick theorem (B2), from (C2) we get—as obtained initially in equation (A2) of reference [39]—that

$$\begin{aligned} &\left\langle (x(t_i + \Delta_n) - x(t_i))^2 (x(t_j + \Delta_n) - x(t_j))^2 \right\rangle \\ &= 4D_H^2 \Delta_n^{4H} + \frac{4D_H^2}{2} (|t_i - t_j - \Delta_n|^{2H} - 2|t_i - t_j|^{2H} + |t_i - t_j + \Delta_n|^{2H}), \end{aligned} \tag{C3}$$

where $t_i - t_j = (i - j) \times \delta t$. From equations (6) and (C2), the EB parameter for this discrete-time FBM scheme can be expressed as

$$\begin{aligned} \text{EB}_{\text{FBM}}^{\text{disc}}(\Delta n) &= \frac{2\delta t}{T - n \times \delta t} + \frac{\delta t^2}{(T - n \times \delta t)^2 n^{4H}} \\ &\times \sum_{k=1}^{\frac{T}{\delta t} - n - 1} (|k - n|^{2H} + |k + n|^{2H} - 2k^{2H})^2 \left(\frac{T}{\delta t} - n - k \right). \end{aligned} \quad (\text{C4})$$

At $k \gg n$, using the Taylor expansion

$$|k - n|^{2H} + |k + n|^{2H} - 2k^{2H} \approx 2H(2H - 1)k^{2H} (n/k)^2, \quad (\text{C5})$$

one can show that for the case $H > 3/4$ the second term in equation (C4) dominates. The sum in this term can be approximated by a continuous integral so that

$$\text{EB}_{\text{FBM}}^{\text{disc}}(\Delta_n) \sim C_2 \times (T/\Delta_n)^{4H-4}, \quad (\text{C6})$$

both for $n = 1$ or $n \gg 1$, that coincides with equation (27), see also figure 4. At $\Delta_1 = \delta t$ and at $H = 0$ from (C4) we obtain expression (34) in the main text, while at $H = 1$ one gets

$$\text{EB}_{\text{FBM}}(\Delta) = 2. \quad (\text{C7})$$

For the Hurst exponents $0 < H \lesssim 1/2$ the first term in expression (C4) dominates and at $\Delta_1 = \delta t$ one gets the approximate expression (36). We checked these theoretical EB predictions at $\Delta_1 = \delta t$ versus FBM-based computer simulations in figure 5. From equation (C4) we also find that at $\Delta_1 = \delta t$ for $H = 1/2$ the EB parameter is

$$\text{EB}_{\text{FBM}}^{\text{disc}}(\Delta_1) \sim 2/(N - 1). \quad (\text{C8})$$

For the case $0 < H < 3/4$ in the limit $n \gg 1$ via approximating the sum in equation (C4) by a continuous integral we obtain

$$\text{EB}_{\text{FBM}}^{\text{disc}}(\Delta_n) \sim \frac{2}{T/\delta t - n} + \frac{n \times C_1(H)}{T/\delta t - n}. \quad (\text{C9})$$

For $H < 3/4$ at $n = 1$ the sum is approximated by the leading term (at $H < 1/2$ only one term is enough). This ansatz works well for small Hurst exponents, while as $H \rightarrow 3/4$ a progressively larger number of terms is to be accounted in the sum for an adequate approximation for the EB parameter. The condition of equality of the first and second term in equation (C9) provides a rough, H -independent estimate for the lag time, see equation (37) in the main text and equation (C10) below, below which the plateau-like, ‘saturation’ behaviour of $\text{EB}_{\text{FBM}}^{\text{disc}}(\Delta)$ is expected to occur. The analytical threshold for this lag time given by equation (37) is plotted in figure 10 versus H and shows that longer saturating regimes of $\text{EB}_{\text{FBM}}^{\text{disc}}(\Delta)$ emerge for smaller H values, consistent with the results of our simulations, as presented in figure 4.

In reality, however, the situation is more involved. If the plateau of EB persists in simulations for a long lag time, the first term in equation (C9) is typically much larger than the second one. This scenario is realised in the region $0 < H < 1/2$ for $\Delta = \Delta_1$. When the Hurst exponent increases and as $H \rightarrow 3/4$ the two terms in equation (C9) become comparable in magnitude. Technically, based on equation (14) and figure 1 of reference [39] both illustrating the behaviour of the coefficient $C_1(H)$ versus H , we find that equating the two

terms in expression (C9) yields in this discrete-time scheme the following condition for the lag time

$$\frac{\Delta_{\text{pl}}^{\text{disc}}(H)}{\delta t} = \frac{\Delta_n}{\delta t} \approx \frac{2}{C_1(H)}. \quad (\text{C10})$$

This gives a universal, δt -independent condition for the critical lag-time value below which the EB plateau is realised. The value of the Hurst exponent via $C_1(H)$ fully controls the EB plateau existence and the lag-time-range over which it persists. Therefore, if

$$C_1(H) \gtrsim 2 \quad (\text{C11})$$

a plateau of $\text{EB}_{\text{FBM}}^{\text{disc}}(\Delta)$ is expected for lag times shorter than the elementary time step, at $\Delta < \delta t$. This effect is thus ‘undetectable’ in our simulations (see figure 4). The condition (C11) is satisfied for large Hurst exponents $1 > H > 3/4$ and also for

$$0.64 \approx H_{\text{pl}} < H < 3/4 \quad (\text{C12})$$

in the region of small H (with $H = 3/4$ being the transition point between ‘large’ and ‘small’ H values). The shaded region in figure 10 demarcates the plateau-containing region of the EB behaviour for canonical FBM. Therefore, in the framework of this discrete-time FBM scheme we conclude using (C10) that at short lag times *no plateau* of $\text{EB}_{\text{FBM}}^{\text{disc}}(\Delta)$ is expected for the Hurst exponents in the range $1 > H \gtrsim H_{\text{pl}}$. This theoretical expectation is supported by the results of our computer simulations presented in figure 4.

Appendix D.

Below, we include additional figures supporting the claims presented in the main text.

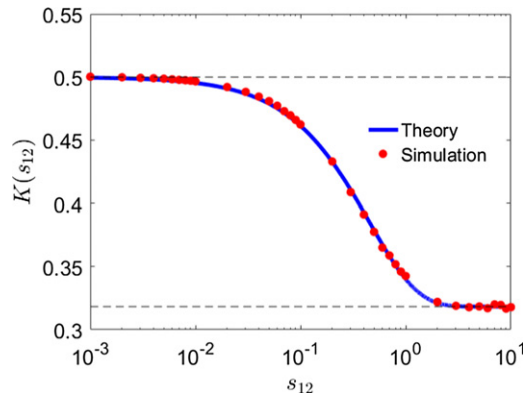


Figure 7. Correlator of the diffusion coefficients (18), as predicted theoretically [132] and calculated from simulations, computed for the same parameters as in Figure 2.

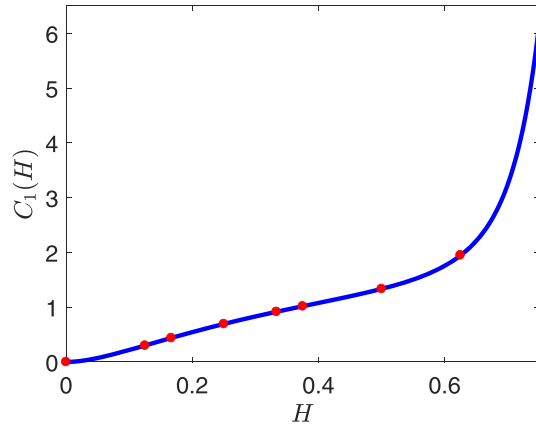


Figure 8. Variation of $C_1(H)$ computed via numerical integration of (31) (blue curve) and results of analytical calculations (red dots). The latter yield $C_1(H) \propto 4\pi^2 H^2$ as the leading-order expansion for (very) small H and the following values for some representative H values: $C_1(1/8) = \frac{8(3\sqrt{2}-4)\Gamma(5/4)^2}{3\sqrt{\pi}} \approx 0.30$, $C_1(1/6) = \frac{11(2^{1/3}-1)\sqrt{\pi}\Gamma(7/3)}{8\Gamma(17/6)} \approx 0.44$, $C_1(1/4) = \log(2) \approx 0.69$, $C_1(1/3) = \frac{27(2-2^{2/3})\sqrt{\pi}\Gamma(11/3)}{80\Gamma(13/6)} \approx 0.91$, $C_1(3/8) = \sqrt{\frac{\pi}{2}} \frac{\Gamma(7/4)}{\Gamma(9/4)} \approx 1.02$, $C_1(1/2) = 4/3 \approx 1.33$, $C_1(5/8) = \frac{(3+\sqrt{2})\sqrt{\pi}\Gamma(9/4)}{2\sqrt{2}\Gamma(11/4)} \approx 1.95$.

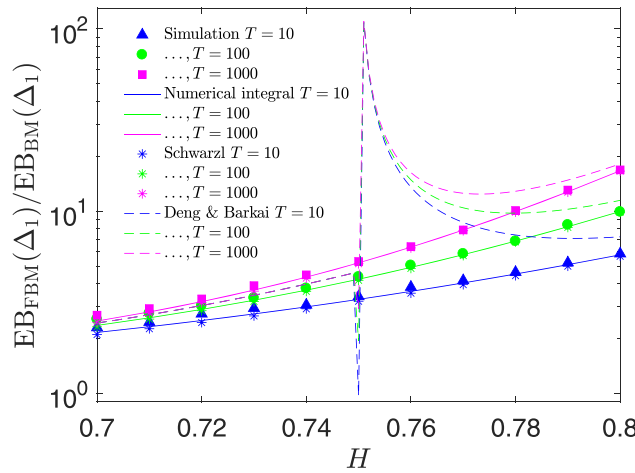


Figure 9. Detailed variation of the normalised EB parameter near the critical point $H = 3/4$. Notations for the curves are the same as in figure 5: the results of computer simulations of FBM equation (8) are the filled symbols, the results of numerical integration of equation (11) of reference [44] are the solid curves, the approximate analytical results of equation (12) of reference [44] are the asterisks and the results of the continuous-time infinite-trajectory-length theory of EB for FBM [39] are the dashed lines. All symbols and lines have the respective colours for varying lengths of the trajectory (see the legend). Other parameters are: $\Delta_1 = 10^{-3}$ and $D_H = 1/2$.

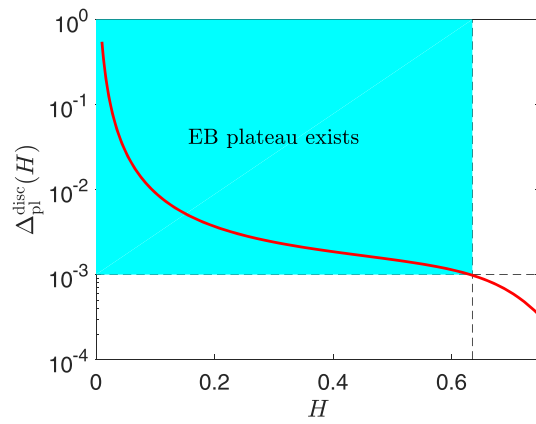


Figure 10. Variation of Δ_{pl}^{disc} for the FBM model, as obtained from equation (37). The Hurst exponent $H_{pl} \approx 0.64$ from equation (C12) and the value of δt are the dotted lines defining the region of existence of a plateau-containing behaviour of $EB_{FBM}(\Delta)$. Parameters: $D_H = 1/2$, $T = 10^2$, and $\delta t = 10^{-3}$.

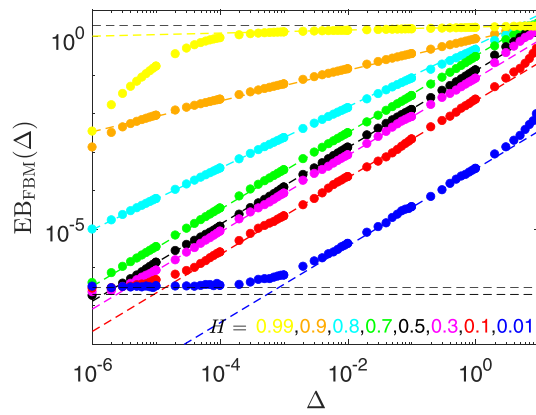


Figure 11. $EB_{FBM}(\Delta)$ is illustrated for the same parameters and the same meaning for the asymptotes as in figure 4, except a smaller time-step ($\delta t = 10^{-6}$) and shorter trace length ($T = 10$) were used here.

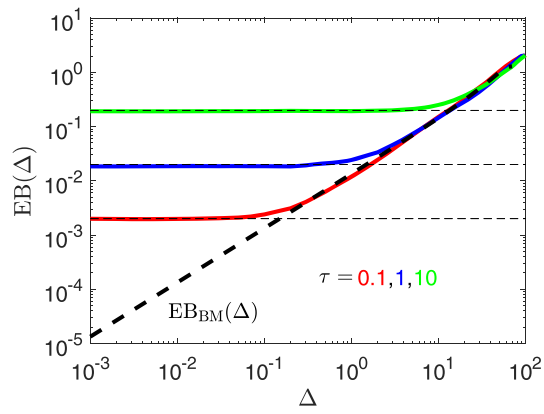


Figure 12. Numerical EB parameter of the DD-FBM process plotted versus the lag time for different DD correlation times, τ . For $\Delta \ll \tau$ the curves approach the plateau value $2\tau/T$ (thin dashed lines). The thick dashed line is the BM asymptote (7). Parameters: $H = 1/5, \sigma = 1, D_H = 1/2, T = 10^2$.

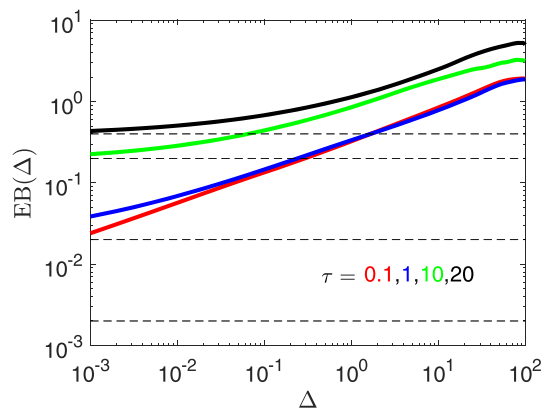


Figure 13. Results of stochastic simulations for the discreteness-induced plateau for $EB_{pl,DD+FBM}$ for varying correlation times (as indicated in the plot). The dashed lines correspond to equation (40). Parameters: $H = 9/10, T = 10^2$.

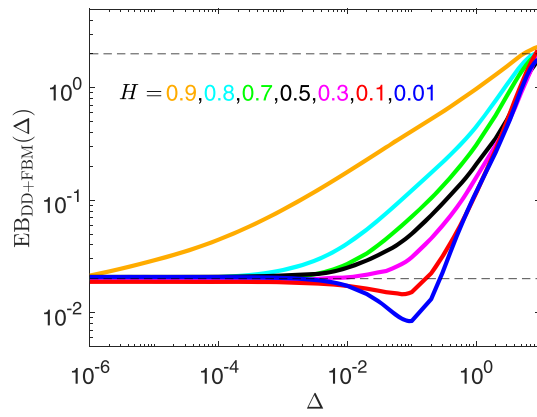


Figure 14. EB parameter for the DD-FBM model, computed for shorter trajectories ($T = 10^1$) and shorter lag-time steps used in simulations ($\delta\Delta = 10^{-6}$), for $\tau = 10^{-1}$. The colour-scheme for the curves and the meaning of the asymptotes are as in figure 6.

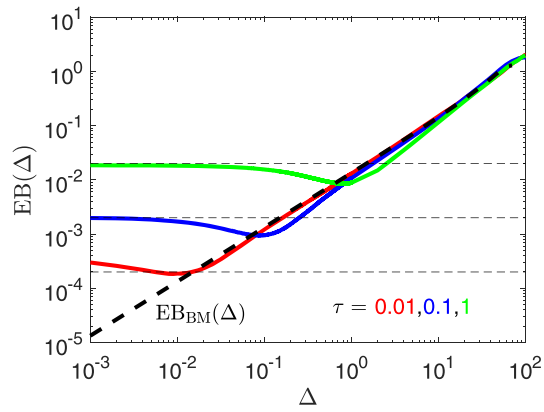


Figure 15. EB for the DD-FBM model obtained by simulations for different values of the DD correlation time τ . The thin dashed lines is the plateau value (40), while the thick dashed line is the EB result for BM, equation (7). Parameters: $H = 1/100$, $T = 10^2$.

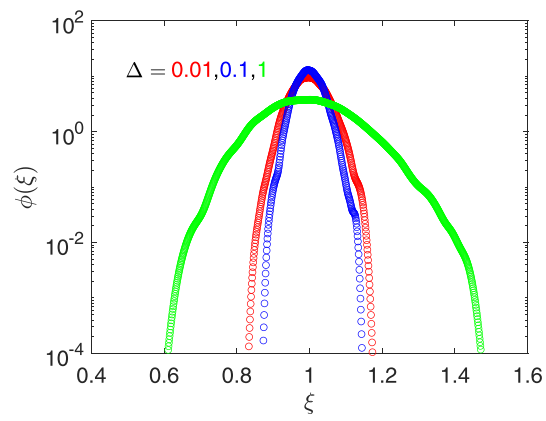


Figure 16. Distributions of individual TAMSDs obtained in our simulations that verify the nonmonotonicity of $EB_{DD+FBM}(\Delta)$ with the lag time for small H values shown in figures 6 and 15. Parameters: $H = 1/100$, $\tau = 0.1$, $\sigma = 1$, $T = 10^2$.

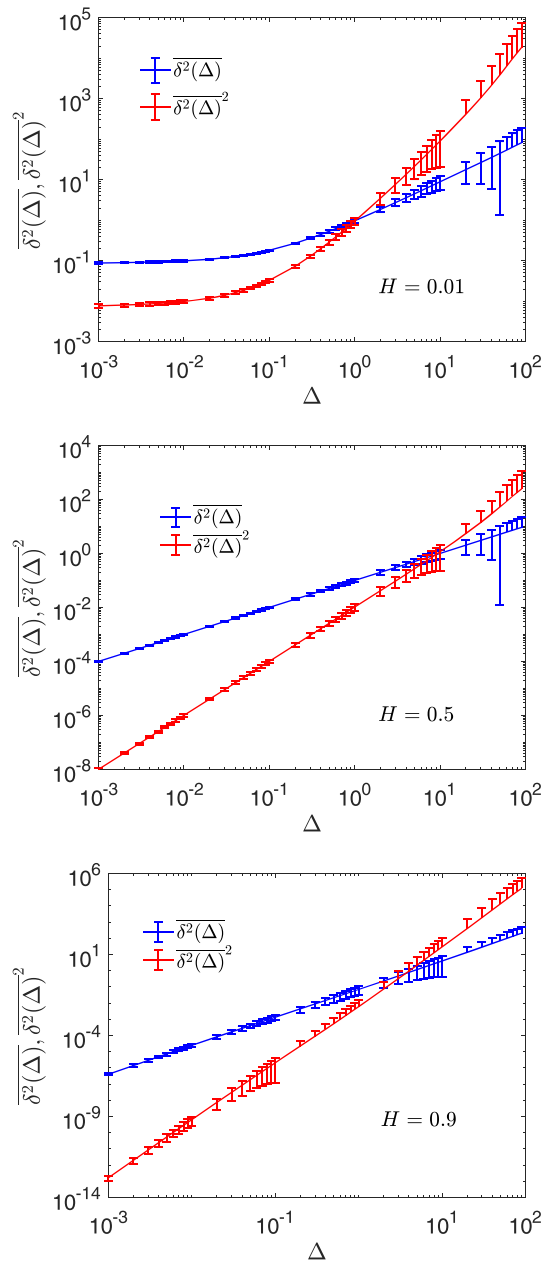


Figure 17. Error bars for the second and fourth moments of the displacement (used for computation of EB, equation (6)) as obtained from our computer simulations. The bars are symmetric about the means (asymmetric in log–log scale). For error bars larger than the mean only the values above the mean are shown in logarithmic scale. Parameters are the same as in figure 6 and $H=1/100, 1/2,$ and $9/10$ (for the graphs from top to bottom, respectively).

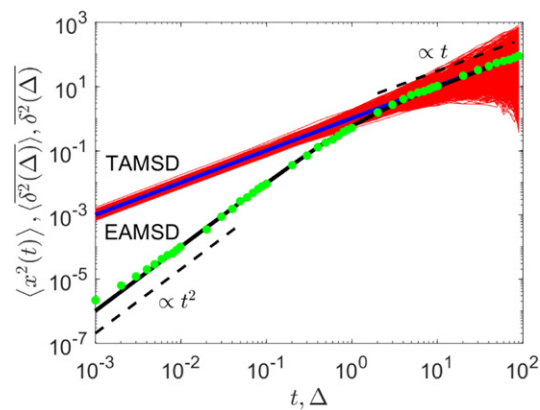


Figure 18. Numerical MSD (filled green circles), analytical MSD (black solid line) and TAMSD (blue solid line), as well as the individual TAMSDs (red curves) for the DD-FBM model with nonequilibrium initial conditions, namely $D(0) = 0$. Parameters: $H = 1/2$, $\tau = 1$, $\sigma = 1$, $D_H = 1/2$, $T = 10^2$.

ORCID iDs

Andrey G Cherstvy  <https://orcid.org/0000-0002-0516-9900>

Samudrajit Thapa  <https://orcid.org/0000-0002-4340-5900>

Ralf Metzler  <https://orcid.org/0000-0002-6013-7020>

References

- [1] Brown R 1828 A brief account of microscopical observations made on the particles contained in the pollen of plants *Phil. Mag.* **4** 161
- [2] Fick A 1855 Über Diffusion *Ann. Phys., Lpz.* **170** 59
- [3] Einstein A 1905 Über die von der molekularkinetischen Theorie der Wärme geforderte Bewegung von in ruhenden Flüssigkeiten suspendierten Teilchen *Ann. Phys., Lpz.* **322** 549
- [4] Sutherland W 1905 A dynamical theory of diffusion for non-electrolytes and the molecular mass of albumin *Phil. Mag.* **9** 781
- [5] Pearson K 1905 The problem of the random walk *Nature* **72** 294
- [6] von Smoluchowski M 1906 Zur kinetischen Theorie der Brownschen Molekularbewegung und der Suspensionen *Ann. Phys., Lpz.* **21** 756
- [7] Langevin P 1908 On the theory of Brownian motion *C. R. Acad. Sci., Paris* **146** 530
- [8] Perrin J 1909 Brownian movement and molecular reality *Ann. Chim. Phys.* **18** 5
- [9] Nordlund I 1914 A new determination of Avogadro's number from Brownian motion of small mercury spherules *Z. Phys. Chem.* **87** 40
- [10] Lévy P 1965 *Processus Stochastiques et Mouvement Brownien* (Paris: Gauthier-Villars)
- [11] Haus J W and Kehr K W 1987 Diffusion in regular and disordered lattices *Phys. Rep.* **150** 263
- [12] Bouchaud J-P and Georges A 1990 Anomalous diffusion in disordered media: statistical mechanisms, models and physical applications *Phys. Rep.* **195** 127
- [13] Havlin S and Ben-Avraham D 2002 Diffusion in disordered media *Adv. Phys.* **51** 187
- [14] Metzler R and Klafter J 2000 The random walk's guide to anomalous diffusion: a fractional dynamics approach *Phys. Rep.* **339** 1

- [15] Metzler R and Klafter J 2004 The restaurant at the end of the random walk: recent developments in the description of anomalous transport by fractional dynamics *J. Phys. A: Math. Gen.* **37** R161
- [16] Burov S, Jeon J-H, Metzler R and Barkai E 2011 Single particle tracking in systems showing anomalous diffusion: the role of weak ergodicity breaking *Phys. Chem. Chem. Phys.* **13** 1800
- [17] Sokolov I M 2012 Models of anomalous diffusion in crowded environments *Soft Matter* **8** 9043
- [18] Höfling F and Franosch T 2013 Anomalous transport in the crowded world of biological cells *Rep. Prog. Phys.* **76** 046602
- [19] Metzler R, Jeon J-H, Cherstvy A G and Barkai E 2014 Anomalous diffusion models and their properties: non-stationarity, non-ergodicity, and ageing at the centenary of single particle tracking *Phys. Chem. Chem. Phys.* **16** 24128
- [20] Meroz Y and Sokolov I M 2015 A toolbox for determining subdiffusive mechanisms *Phys. Rep.* **573** 1
- [21] Norregaard K, Metzler R, Ritter C M, Berg-Sørensen K and Oddershede L B 2017 Manipulation and motion of organelles and single molecules in living cells *Chem. Rev.* **117** 4342
- [22] Metzler R 2019 Brownian motion and beyond: first-passage, power spectrum, non-Gaussianity, and anomalous diffusion *J. Stat. Mech.* **114003**
- [23] Krapf D and Metzler R 2019 Strange interfacial molecular dynamics *Phys. Today* **72** 48
- [24] Golding I and Cox E C 2006 Physical nature of bacterial cytoplasm *Phys. Rev. Lett.* **96** 098102
- [25] Weber S C, Spakowitz A J and Theriot J A 2010 Bacterial chromosomal loci move subdiffusively through a viscoelastic cytoplasm *Phys. Rev. Lett.* **104** 238102
- [26] di Rienzo C, Piazza V, Gratton E, Beltram F and Cardarelli F 2014 Probing short-range protein Brownian motion in the cytoplasm of living cells *Nat. Commun.* **5** 5891
- [27] Jeon J-H, Tejedor V, Burov S, Barkai E, Selhuber-Unke C, Berg-Sørensen K, Oddershede L and Metzler R 2011 *In vivo* anomalous diffusion and weak ergodicity breaking of lipid granules *Phys. Rev. Lett.* **106** 048103
- [28] Stachura S and Kneller G R 2015 Communication: probing anomalous diffusion in frequency space *J. Chem. Phys.* **143** 191103
- [29] He Y, Burov S, Metzler R and Barkai E 2008 Random time-scale invariant diffusion and transport coefficients *Phys. Rev. Lett.* **101** 058101
- [30] Jeon J-H, Monne H M, Javanainen M and Metzler R 2012 Anomalous diffusion of phospholipids and cholesterol in a lipid bilayer and its origins *Phys. Rev. Lett.* **109** 188103
- [31] Bressloff P C and Newby J M 2013 Stochastic models of intracellular transport *Rev. Mod. Phys.* **85** 135
- [32] Goychuk I 2018 Viscoelastic subdiffusion in a random Gaussian environment *Phys. Chem. Chem. Phys.* **20** 24140
- [33] Liu S-L, Wang Z-G, Xie H-Y, Liu A-A, Lamb D C and Pang D-W 2020 Single-virus tracking: from imaging methodologies to virological applications *Chem. Rev.* **3** 1936
- [34] Montroll E W and Weiss G H 1965 Random walks on lattices. II *J. Math. Phys.* **6** 167
- [35] Tabei S M A, Burov S, Kim H Y, Kuznetsov A, Huynh T, Jureller J, Philipson L H, Dinner A R and Scherer N F 2013 Intracellular transport of insulin granules is a subordinated random walk *Proc. Natl Acad. Sci. USA* **110** 4911
- [36] Akimoto T, Yamamoto E, Yasuoka K, Hirano Y and Yasui M 2011 Non-Gaussian fluctuations resulting from power-law trapping in a lipid bilayer *Phys. Rev. Lett.* **107** 178103
- [37] Kolmogorov A N 1940 Wiener'sche Spiralen und einige andere interessante Kurven im Hilbertschen Raum *C. R. Acad. Sci., Paris* **26** 115
- [38] Mandelbrot B B and Van Ness J W 1968 Fractional Brownian motions, fractional noises and applications *SIAM Rev.* **10** 422
- [39] Deng W H and Barkai E 2009 Ergodic properties of fractional Brownian-Langevin motion *Phys. Rev. E* **79** 011112
- [40] Wada A H O and Vojta T 2018 Fractional Brownian motion with a reflecting wall *Phys. Rev. E* **97** 020102
- [41] Delorme M and Wiese K J 2016 Perturbative expansion for the maximum of fractional Brownian motion *Phys. Rev. E* **97** 012134
- [42] Jeon J-H and Metzler R 2010 Fractional Brownian motion and motion governed by the fractional Langevin equation in confined geometries *Phys. Rev. E* **81** 021103
- [43] Jeon J-H and Metzler R 2012 Inequivalence of time and ensemble averages in ergodic systems: exponential versus power-law relaxation in confinement *Phys. Rev. E* **85** 021147

- [44] Schwarzl M, Godec A and Metzler R 2017 Quantifying non-ergodicity of anomalous diffusion with higher order moments *Sci. Rep.* **7** 3878
- [45] Meerschaert M M and Sabzikar F 2013 Tempered fractional Brownian motion *Stat. Probab. Lett.* **83** 2269
- [46] Molina-Garcia D, Sandev T, Safdari H, Pagnini G, Chechkin A V and Metzler R 2018 Crossover from anomalous to normal diffusion: truncated power-law noise correlations and applications to dynamics in lipid bilayers *New J. Phys.* **20** 103027
- [47] Cherstvy A G, Chechkin A V and Metzler R 2013 Anomalous diffusion and ergodicity breaking in heterogeneous diffusion processes *New J. Phys.* **15** 083039
- [48] Cherstvy A G and Metzler R 2013 Population splitting, trapping, and non-ergodicity in heterogeneous diffusion processes *Phys. Chem. Chem. Phys.* **15** 20220
- [49] Cherstvy A G, Chechkin A V and Metzler R 2014 Ageing and confinement in non-ergodic heterogeneous diffusion processes *J. Phys. A: Math. Theor.* **47** 485002
- [50] Cherstvy A G and Metzler R 2014 Nonergodicity, fluctuations, and criticality in heterogeneous diffusion processes *Phys. Rev. E* **90** 012134
- [51] Cherstvy A G and Metzler R 2015 Ergodicity breaking, ageing, and confinement in generalized diffusion processes with position and time dependent diffusivity *J. Stat. Mech.* P05010
- [52] Heidernätsch M 2015 On the diffusion in inhomogeneous systems *PhD Thesis* TU Chemnitz
- [53] Leibovich N and Barkai E 2019 Infinite ergodic theory for heterogeneous diffusion processes *Phys. Rev. E* **99** 042138
- [54] Wang B, Guo J, Bae S C and Granick S 2012 When Brownian diffusion is not Gaussian *Nat. Mater.* **11** 481
- [55] Wang B, Anthony S M, Bae S C and Granick S 2009 Anomalous yet Brownian *Proc. Natl Acad. Sci. USA* **106** 15160
- [56] Chaudhuri P, Berthier L and Kob W 2007 Universal nature of particle displacements close to glass and jamming transitions *Phys. Rev. Lett.* **99** 060604
- [57] Roldan-Vargas S, Rovigatti L and Sciortino F 2017 Connectivity, dynamics, and structure in a tetrahedral network liquid *Soft Matter* **13** 514
- [58] Samanta N and Chakrabarti R 2016 Tracer diffusion in a sea of polymers with blinding zones: mobile versus frozen traps *Soft Matter* **12** 8554
- [59] Toyota T, Head D A, Schmidt C F and Mizuno D 2011 Non-Gaussian athermal fluctuations in active gels *Soft Matter* **7** 3234
- [60] Silva M S, Stuhmann B, Betz T and Koenderink G H 2014 Time-resolved microrheology of actively remodeling actomyosin in networks *New J. Phys.* **16** 075010
- [61] Valentine M T, Kaplan P D, Thota D, Crocker J C, Gisler T, Prudhomme R K, Beck M and Weitz D A 2001 Investigating the microenvironments of inhomogeneous soft materials with multiple particle tracking *Phys. Rev. E* **64** 061506
- [62] Weeks E R, Crocker J C, Levitt A C, Schofield A and Weitz D A 2000 Three-dimensional direct imaging of structural relaxation near the colloidal glass transition *Science* **287** 627
- [63] Kegel W K and van Blaaderen A 2000 Direct observation of dynamical heterogeneities in colloidal hard-sphere suspensions *Science* **287** 290
- [64] Leptos K C, Guasto J S, Gollub J P, Pesci A I and Goldstein R E 2009 Dynamics of enhanced tracer diffusion in suspensions of swimming eukaryotic microorganisms *Phys. Rev. Lett.* **103** 198103
- [65] Beck C and Cohen E D B 2003 Superstatistics *Physica A* **322** 267
- [66] Beck C 2006 Superstatistical Brownian motion *Prog. Theor. Phys. Suppl.* **162** 29
- [67] Chubynsky M V and Slater G W 2014 Diffusing diffusivity: a model for anomalous yet Brownian diffusion *Phys. Rev. Lett.* **113** 098302
- [68] Heidernätsch M, Bauer M and Radons G 2013 Characterizing N-dimensional anisotropic Brownian motion by the distribution of diffusivities *J. Chem. Phys.* **139** 184105
- [69] Bauer M, Valiullin R, Radons G and Kärger J 2011 How to compare diffusion processes assessed by single-particle tracking and pulsed field gradient nuclear magnetic resonance *J. Chem. Phys.* **135** 144118
- [70] Spakowitz A J 2019 Transient anomalous diffusion in a heterogeneous environment *Front. Phys.* **7** 119
- [71] Chakraborty I and Roichman Y 2020 Disorder-induced Fickian, yet non-Gaussian diffusion in heterogeneous media *Phys. Rev. Res.* **2** 022020

- [72] Mark C 2018 Heterogeneous stochastic processes in complex dynamic systems *PhD Thesis* Friedrich-Alexander-Universität Erlangen-Nürnberg
- [73] Luo L and Yi M 2018 Non-Gaussian diffusion in static disordered media *Phys. Rev. E* **97** 042122
- [74] Wolfson M, Liepold C, Lin B and Rice S A 2018 A comment on the position dependent diffusion coefficient representation of structural heterogeneity *J. Chem. Phys.* **148** 194901
- [75] Ślęzak J and Burov S 2019 From diffusion in compartmentalized media to non-Gaussian random walks (arXiv:1909.11395)
- [76] Jain R and Sebastian K L 2016 Diffusion in a crowded, rearranging environment *J. Phys. Chem. B* **120** 3988
- [77] Jain R and Sebastian K L 2017 Diffusing diffusivity: a new derivation and comparison with simulations *J. Chem. Sci.* **126** 929
- [78] Jain R and Sebastian K L 2018 Diffusing diffusivity: fractional Brownian oscillator model for subdiffusion and its solution *Phys. Rev. E* **98** 052138
- [79] Tyagi N and Cherayil B J 2017 Non-Gaussian Brownian diffusion in dynamically disordered thermal environments *J. Phys. Chem. B* **121** 7204
- [80] Uneyama T, Miyaguchi T and Akimoto T 2015 Fluctuation analysis of time-averaged mean-square displacement for the Langevin equation with time-dependent and fluctuating diffusivity *Phys. Rev. E* **92** 032140
- [81] Miyaguchi T, Akimoto T and Yamamoto E 2016 Langevin equation with fluctuating diffusivity: a two-state model *Phys. Rev. E* **94** 012109
- [82] Akimoto T and Yamamoto E 2016 Distributional behaviors of time-averaged observables in the Langevin equation with fluctuating diffusivity: normal diffusion but anomalous fluctuations *Phys. Rev. E* **93** 062109
- [83] Miyaguchi T 2017 Elucidating fluctuating diffusivity in center-of-mass motion of polymer models with time-averaged mean-square-displacement tensor *Phys. Rev. E* **96** 042501
- [84] Miyaguchi T, Uneyama T and Akimoto T 2019 Brownian motion with alternately fluctuating diffusivity: stretched-exponential and power-law relaxation *Phys. Rev. E* **100** 012116
- [85] Uneyama T, Miyaguchi T and Akimoto T 2019 Relaxation functions of the Ornstein-Uhlenbeck process with fluctuating diffusivity *Phys. Rev. E* **99** 032127
- [86] Cherstvy A G and Metzler R 2016 Anomalous diffusion in time-fluctuating non-stationary diffusivity landscapes *Phys. Chem. Chem. Phys.* **18** 23840
- [87] Chechkin A V, Seno F, Metzler R and Sokolov I M 2017 Brownian yet non-Gaussian diffusion: from superstatistics to subordination of diffusing diffusivities *Phys. Rev. X* **7** 021002
- [88] Sposini V, Chechkin A V, Seno F, Pagnini G and Metzler R 2018 Random diffusivity from stochastic equations: comparison of two models for Brownian yet non-Gaussian diffusion *New J. Phys.* **20** 043044
- [89] Sposini V, Chechkin A V and Metzler R 2019 First passage statistics for diffusing diffusivity *J. Phys. A: Math. Theor.* **52** 04LT01
- [90] Ślęzak J, Metzler R and Magdziarz M 2019 Codifference can detect ergodicity breaking and non-Gaussianity *New J. Phys.* **21** 053008
- [91] Mackala A and Magdziarz M 2019 Statistical analysis of superstatistical fractional Brownian motion and applications *Phys. Rev. E* **99** 012143
- [92] Hidalgo-Soria M and Barkai E 2020 The Hitchhiker model for Laplace diffusion processes in the cell environment *Phys. Rev. E* **102** 012109
- [93] Barkai E and Burov S 2020 Packets of diffusing particles exhibit universal exponential tails *Phys. Rev. Lett.* **124** 060603
- [94] Postnikov E B, Chechkin A V and Sokolov I M 2020 Brownian yet non-Gaussian diffusion in heterogeneous media: from superstatistics to homogenization *New J. Phys.* **22** 063046
- [95] Lanoiselee Y, Moutal N and Grebenkov D S 2018 Diffusion-limited reactions in dynamic heterogeneous media *Nat. Commun.* **9** 4398
- [96] Lanoiselee Y and Grebenkov D S 2018 A model of non-Gaussian diffusion in heterogeneous media *J. Phys. A: Math. Theor.* **51** 145602
- [97] Lanoiselee Y and Grebenkov D S 2019 Non-Gaussian diffusion of mixed origins *J. Phys. A: Math. Theor.* **52** 304001
- [98] Grebenkov D S 2019 Time-averaged mean square displacement for switching diffusion *Phys. Rev. E* **99** 032133

- [99] Lampo T J, Stylianidou S, Backlund M P, Wiggins P A and Spakowitz A J 2017 Cytoplasmic RNA-protein particles exhibit non-Gaussian subdiffusive behavior *Biophys. J.* **112** 532
- [100] Jeon J-H, Javanainen M, Martinez-Seara H, Metzler R and Vattulainen L 2016 Protein crowding in lipid bilayers gives rise to non-Gaussian anomalous lateral diffusion of phospholipids and proteins *Phys. Rev. X* **6** 021006
- [101] Ślęzak J, Metzler R and Magdziarz M 2018 Superstatistical generalised Langevin equation: non-Gaussian viscoelastic anomalous diffusion *New J. Phys.* **20** 023026
- [102] Ślęzak J, Burnecki K and Metzler R 2019 Random coefficient autoregressive processes describe Brownian yet non-Gaussian diffusion in heterogeneous systems *New J. Phys.* **21** 073056
- [103] Metzler R, Jeon J-H and Cherstvy A G 2016 Non-Brownian diffusion in lipid membranes: experiments and simulations *Biochim. Biophys. Acta Biomembr.* **1858** 2451
- [104] Yamamoto E, Akimoto T, Kalli A C, Yasuoka K and Sansom M S P 2017 Dynamic interactions between a membrane binding protein and lipids induce fluctuating diffusivity *Sci. Adv.* **3** e1601871
- [105] Wagner C E, Turner B S, Rubinstein M, McKinley G H and Ribbeck K 2017 A rheological study of the association and dynamics of MUC5AC gels *Biomacromolecules* **18** 3654
- [106] Skaug M J, Mabry J and Schwartz D K 2013 Intermittent molecular hopping at the solid-liquid interface *Phys. Rev. Lett.* **110** 256101
- [107] Skaug M J, Mabry J N and Schwartz D K 2014 Single-molecule tracking of polymer surface diffusion *J. Am. Chem. Soc.* **136** 1327
- [108] Cherstvy A G, Thapa S, Wagner C E and Metzler R 2019 Non-Gaussian, non-ergodic, and non-Fickian diffusion of tracers in mucin hydrogels *Soft Matter* **15** 2481
- [109] Cherstvy A G, Nagel O, Beta C and Metzler R 2018 Non-Gaussianity, population heterogeneity, and transient superdiffusion in the spreading dynamics of amoeboid cells *Phys. Chem. Chem. Phys.* **20** 23034
- [110] Witzel P, Götz M, Lanoiselee Y, Fransoch T, Grebenkov D S and Heinrich D 2019 Heterogeneities shape passive intracellular transport *Biophys. J.* **117** 203
- [111] Matse M, Chubynsky M V and Bechhoefer J 2017 Test of the diffusing-diffusivity mechanism using near-wall colloidal dynamics *Phys. Rev. E* **96** 042604
- [112] Cuetos A, Morillo N and Patti A 2018 Fickian yet non-Gaussian diffusion is not ubiquitous in soft matter *Phys. Rev. E* **98** 042129
- [113] Li Y, Marchesoni F, Debnath D and Ghosh P K 2019 Non-Gaussian normal diffusion in a fluctuating corrugated channel *Phys. Rev. Res.* **1** 033003
- [114] He W, Song H, Su Y, Geng L, Ackerson B J, Peng H B and Tong P 2016 Dynamic heterogeneity and non-Gaussian statistics for acetylcholine receptors on live cell membrane *Nat. Commun.* **7** 11701
- [115] Barkai E, Garini Y and Metzler R 2012 Strange kinetics of single molecules in living cells *Phys. Today* **65** 29
- [116] Bouchaud J-P 1992 Weak ergodicity breaking and aging in disordered systems *J. Physique I* **2** 1705
- [117] Andereanov A and Grebenkov D S 2012 Time-averaged MSD of Brownian motion *J. Stat. Mech.* P07001
- [118] Hou R, Cherstvy A G, Metzler R and Akimoto T 2018 Biased continuous-time random walks for ordinary and equilibrium cases: facilitation of diffusion, ergodicity breaking and ageing *Phys. Chem. Chem. Phys.* **20** 20827
- [119] Budini A A 2017 Memory-induced diffusive-superdiffusive transition: ensemble and time-averaged observables *Phys. Rev. E* **95** 052110
- [120] Cherstvy A G, Thapa S, Mardoukhi Y, Chechkin A V and Metzler R 2018 Time averages and their statistical variation for the Ornstein-Uhlenbeck process: role of initial particle conditions and relaxation to stationarity *Phys. Rev. E* **98** 022134
- [121] Burov S, Metzler R and Barkai E 2010 Aging and nonergodicity beyond the Khinchin theorem *Proc. Natl Acad. Sci. USA* **107** 13228
- [122] Lebowitz J L and Penrose O 1973 Modern ergodic theory *Phys. Today* **26** 23
- [123] Jeon J-H, Barkai E and Metzler R 2013 Noisy continuous time random walks *J. Chem. Phys.* **139** 121916
- [124] Jeon J-H, Leijnse N, Oddershede L and Metzler R 2013 Anomalous diffusion and power-law relaxation in wormlike micellar solution *New J. Phys.* **15** 045011

- [125] Ghosh S K, Cherstvy A G and Metzler R 2015 Non-universal tracer diffusion in crowded media of non-inert obstacles *Phys. Chem. Chem. Phys.* **17** 1847
- [126] Krapf D et al 2019 Spectral content of a single non-Brownian trajectory *Phys. Rev. X* **9** 011019
- [127] Sposini V, Metzler R and Oshanin G 2019 Single-trajectory spectral analysis of scaled Brownian motion *New J. Phys.* **21** 073043
- [128] Sposini V, Grebenkov D S, Metzler R, Oshanin G and Seno F 2020 Universal spectral features of different classes of random-diffusivity processes *New J. Phys.* **22** 063056
- [129] Uhlenbeck G E and Ornstein L S 1930 On the theory of the Brownian motion *Phys. Rev.* **36** 823
- [130] Wang W, Seno F, Sokolov I M, Chechkin A V and Metzler R 2020 Unexpected crossovers in correlated random-diffusivity processes *New J. Phys.* **22** 083041
- [131] Schulz J H P, Barkai E and Metzler R 2013 Aging effects and population splitting in single-particle trajectory averages *Phys. Rev. Lett.* **110** 020602
- [132] Schulz J H P, Barkai E and Metzler R 2014 Aging renewal theory and application to random walks *Phys. Rev. X* **4** 011028
- [133] Martin D S, Forstner M B and Käs J A 2002 Apparent subdiffusion inherent to single particle tracking *Biophys. J.* **83** 2109
- [134] Weiss M 2019 Resampling single-particle tracking data eliminates localization errors and reveals proper diffusion anomalies *Phys. Rev. E* **100** 042125
- [135] Li M, Sentissi O, Azzini S, Schnoering G, Canaguier-Durand A and Genet C 2019 Subfemtonewton force fields measured with ergodic Brownian ensembles *Phys. Rev. A* **100** 063816
- [136] Safdari H, Cherstvy A G, Chechkin A V, Thiel F, Sokolov I M and Metzler R 2015 Quantifying the non-ergodicity of scaled Brownian motion *J. Phys. A: Math. Theor.* **48** 375002
- [137] Grebenkov D S 2013 Optimal and suboptimal quadratic forms for noncentered Gaussian processes *Phys. Rev. E* **88** 032140
- [138] Kärger J 1985 NMR self-diffusion studies in heterogeneous systems *Adv. Colloid Interface Sci.* **23** 129
- [139] Fieremans E, Novikov D S, Jensen J H and Helpert J A 2010 Monte Carlo study of a two-compartment exchange model of diffusion *NMR Biomed.* **23** 711
- [140] Novikov D S, Fieremans E, Jespersen S N and Kiselev V G 2019 Quantifying brain microstructure with diffusion MRI: theory and parameter estimation *NMR Biomed.* **32** e3998